Probing the correlation between ligand efficacy and conformational diversity at the α_{1A}-adrenoreceptor reveals allosteric coupling of its microswitches

Received for publication, January 31, 2020, and in revised form, April 14, 2020 Published, Papers in Press, April 17, 2020, DOI 10.1074/jbc.RA120.012842

Feng-Jie Wu[‡§¶], Lisa M. Williams[¶], Alaa Abdul-Ridha[¶], Avanka Gunatilaka[¶], Tasneem M. Vaid[‡§¶], Martina Kocan[¶], Alice R. Whitehead[¶], Michael D. W. Griffin[‡§], Ross A. D. Bathgate[‡¶], Daniel J. Scott[‡¶1], and Paul R. Gooley[‡§2]

From the [‡]Department of Biochemistry and Molecular Biology, University of Melbourne, Parkville 3052, VIC, Australia, the [§]Bio21 Molecular Science and Biotechnology Institute, University of Melbourne, Parkville 3052, VIC, Australia and [¶]The Florey Institute of Neuroscience and Mental Health, University of Melbourne, Parkville 3052, VIC, Australia

Edited by Henrik G. Dohlman

G protein–coupled receptors (GPCRs) use a series of conserved microswitches to transmit signals across the cell membrane via an allosteric network encompassing the ligand-binding site and the G protein-binding site. Crystal structures of GPCRs provide snapshots of their inactive and active states, but poorly describe the conformational dynamics of the allosteric network that underlies GPCR activation. Here, we analyzed the correlation between ligand binding and receptor conformation of the α_{1A}-adrenoreceptor, a GPCR that stimulates smooth muscle contraction in response to binding noradrenaline. NMR of [$^{13}C^{\epsilon}H_3$]methionine-labeled α_{1A}-adrenoreceptor variants, each exhibiting differing signaling capacities, revealed how different classes of ligands modulate the conformational equilibria of this receptor. [$^{13}C^{\epsilon}H_3$]Methionine residues near the microswitches exhibited distinct states that correlated with ligand efficacies, supporting a conformational selection mechanism. We propose that allosteric coupling among the microswitches controls the conformation of the α_{1A}-adrenoreceptor and underlies the mechanism of ligand modulation of GPCR signaling in cells.

G protein–coupled receptors (GPCRs)[3] are integral membrane proteins sharing a common seven-helix transmembrane domain (TMD). Conformational changes to the TMD are required to transmit the extracellular stimuli intracellularly to activate signaling pathways. Over the past 20 years X-ray crystal structures, and more recently cryo-EM structures, have revealed a plethora of structural details on how functionally different ligands interact with GPCRs and the conformational changes they induce. Most structures solved to date are of GPCRs in inactive states, bound to inverse agonists or antagonists (1). A few have been crystalized with agonist alone (1), with resultant structures similar to antagonist-bound inactive states. Complexes of GPCRs with active state-stabilizing nanobodies, engineered mini G proteins, Gα C-terminal peptide, or heterotrimeric G proteins appear necessary to stabilize agonist-bound GPCRs in active states for X-ray and cryoelectron microscopy structure determination (2). Using these tools, several active state GPCR structures have been solved (1–3), revealing conserved conformational changes that occur upon receptor activation. These include rearrangements in the ligand-binding site and a large outward movement at the cytoplasmic side of transmembrane (TM) helix 6 (TM6) to accommodate G protein binding. Although providing a wealth of structural detail of static receptor conformations, these structures generally do not provide insight into GPCR signaling complexities such as basal receptor activity, partial agonism, and biased agonism.

To address this shortfall, spectroscopic techniques, supported by molecular dynamic simulations, have given insight into the conformational dynamics that underlie the activity of a few diffusible ligand-activated GPCRs including β_2-adrenergic receptor (β_2-AR) (4–12), β_1-adrenergic receptor (β_1-AR) (13, 14), adenosine A_{2A} receptor ($A_{2A}R$) (15–18), μ-opioid receptor (μOR) (19, 20), leukotriene B4 receptor (BLT2) (21), and the M2 muscarinic acetylcholine receptor (M2R) (22). By far the most studied receptor in this regard is β_2-AR, for which [$^{13}C^{\epsilon}H_3$]methionine labeling NMR (5, 8, 9), ^{19}F NMR (6, 7, 10, 11), and electron paramagnetic resonance (10) have been applied to characterize the conformational signatures of this receptor when bound to various ligands and a G protein mimetic nanobody. These studies reveal that GPCRs are highly dynamic, sampling inactive and active conformational states, and are thought to predominantly function via a conformational selection mechanism (15, 23). Such a mechanism posits that a GPCR constantly samples various

This work was supported by National Health and Medical Research Council (NHMRC) project Grants 1081801 (to D. J. S.), 1081844 (to P. R. G., D. J. S., and R. A. D. B.), and 1141034 (to D. J. S., P. R. G., and R. A. D. B.), and a NHMRC Boosting Dementia Research Leadership Fellowship (to D. J. S.). The authors declare that they have no conflicts of interest with the contents of this article.

This article contains Figs. S1–S11 and Table S1.

[1] To whom correspondence may be addressed: The Florey Institute of Neuroscience and Mental Health, The University of Melbourne, Melbourne, Australia. Tel.: 61-0-3-9035-7584; E-mail: daniel.scott@florey.edu.au.

[2] To whom correspondence may be addressed: Dept. of Biochemistry and Molecular Biology, The University of Melbourne, Bio21 Molecular Science and Biotechnology Institute. Tel.: 61-0-3-8344-2273; E-mail: prg@unimelb.edu.au.

[3] The abbreviations used are: GPCR, G protein–coupled receptors; β_2-AR, β_2-adrenergic receptor; μ-OR, μ-opioid receptor; BPH, benign prostatic hyperplasia; DDM, *n*-dodecyl-β-D-maltopyranoside; HMQC, heteronuclear multiple quantum coherence; MD, molecular dynamics; TMD, transmembrane domain; IP, inositol phosphate; DMEM, Dulbecco's modified Eagle's medium; FBS, fetal bovine serum; QAPB, quinazoline piperazine BODIPY; PDB, Protein Data Bank; α_{1A}-AR, α_{1A}-adrenoreceptor.

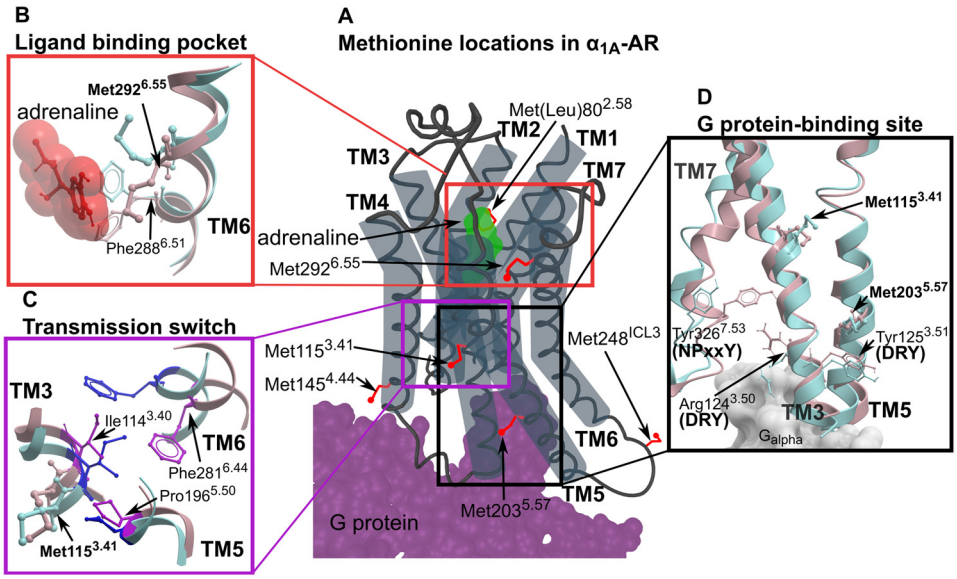

Figure 1. Methionine residues in α_{1A}-AR. *A,* the location of six methionines on a cartoon representation of α_{1A}-AR. Methionine side chains are highlighted as *red sticks*. Bound adrenaline and G protein are colored in *green* and *purple*, respectively. *B–D,* homology models of α_{1A}-AR-A4 in the inactive state (*blue*; modeled on the X-ray crystal structure of inactive β_2-AR, PDB ID 5JQH) and active state (*pink*; modeled on the X-ray crystal structure of active β_2-AR, PDB ID 3SN6) are superimposed showing inferred conformational changes that occur in the ligand-binding pocket (*B*), transmission switch (*C*), and G protein-binding site (*D*).

inactive and active conformations, all existing in equilibrium. Ligands preferentially bind to particular receptor states, depending on their pharmacological characteristics, thus shifting the conformational equilibrium toward these preferred states and modulating the signaling output of the system. The extracellular orthosteric ligand-binding site in adrenoceptors is connected to the intracellular G protein-binding site through a series of conserved microswitches (24–27) (Fig. 1): a central transmission switch (also called the connector region, CW*X*P motif or PIF motif (28)), the NP*XX*Y switch, and the intracellular G protein-binding site, characterized by the DRY motif (or switch). How these microswitches coordinate the transmission of the extracellular signal is not clear, but molecular dynamics (MD) simulations and NMR data have led to a mechanistic description of "loose allosteric coupling" (28).

This mechanism refers to each microswitch as conformationally independent from the others, which as an active DRY motif state is not significantly dependent on an active state in the transmission switch. That said, an active state in the transmission switch does increase the probability of the DRY motif (and thus the receptor) to sample active states (thus, loose allosteric coupling) (28). Put simply, the conformational changes that occur in the microswitches are thought to drive the overall equilibrium state of the receptor system. Despite recent work, it is not well-understood how the binding of ligands such as inverse agonists influence the microswitch state equilibria to decrease basal receptor activity.

α_1-Adrenoceptors (α_1-ARs) comprise three G_q-coupled GPCR subtypes (α_{1A}-, α_{1B}-, and α_{1D}-AR) that bind and sense the endogenous catecholamines, adrenaline and noradrenaline, to modulate a range of physiological processes. In the periphery, postsynaptic α_1-AR stimulation by catecholamines mediates smooth muscle contraction, thus α_1-AR antagonists and inverse agonists are clinically prescribed to treat hypertension and benign prostatic hyperplasia (BPH) (29). α_1-ARs are also widely expressed in the central nervous system, but the lack of subtype-selective antibodies and ligands limits the understanding of their role in neuroplasticity and neurodegeneration (30). Currently there are no available crystal structures of an α_1-AR family member, which limits the rational design of more selective compounds to probe the physiological role of α_{1A}-adrenoreceptor (α_{1A}-AR) in the central nervous system.

Recombinant α_{1A}-AR expresses poorly and the resultant protein is particularly unstable when purified in detergent (31), which has hindered biochemical studies of this GPCR. Recently, we engineered an α_{1A}-AR variant, α_{1A}-AR-A4, that can be expressed in *Escherichia coli* and exhibits improved stability when purified in detergents (32). When expressed in COS-7 cells α_{1A}-AR-A4 exhibits no signaling efficacy in response to adrenaline stimulation (32). In the present study, α_{1A}-AR-A4 was labeled with [$^{13}C^{\epsilon}H_3$]methionine at the five naturally occurring methionine residues, providing NMR probes to assess how inverse agonists, partial agonists, and full agonists influence receptor conformational equilibria. Three of these methionines are excellent probes of the ligand-binding site and the microswitches proposed to be markers of signal transmission: Met-292$^{6.55}$ (superscript denotes GPCRdb numbering (33)) is located in the ligand-binding site; Met-115$^{3.41}$ is proximal to the transmission switch (Ile-114$^{3.40}$, Pro-196$^{5.50}$, Leu-197$^{5.51}$, Phe-281$^{6.44}$, and Trp-285$^{6.48}$); and Met-203$^{5.57}$ sits above the tyrosine of the DRY motif (Asp-130$^{3.49}$, Arg-131$^{3.50}$, and Tyr-132$^{3.51}$). Using the inactive α_{1A}-AR variant, α_{1A}-AR-A4, and by reverse mutation to an active receptor (α_{1A}-AR-A4–active) we show that for Met-115$^{3.41}$ and Met-203$^{5.57}$ the chemical shifts and line widths of the $^{13}C^{\epsilon}H_3$ groups are dependent on ligand efficacy (from strong inverse agonist to full agonist), suggesting that α_{1A}-AR activation proceeds primarily through a conformational selection mechanism.

Results

$^{13}C^{\epsilon}H_3$ Methionine labeling and NMR signal assignment

α_{1A}-AR-A4 is a thermostabilized variant of the human α_{1A}-AR that contains 15 amino acid substitutions over wildtype (WT) human α_{1A}-AR (Fig. S1). Excluding Met-1, α_{1A}-AR-A4 possesses six methionine residues, five of which are naturally occurring (Met-115$^{3.41}$, Met-145$^{4.44}$, Met-203$^{5.57}$, Met-248^{ICL3}, and Met-292$^{6.55}$) and one, Met-80$^{2.58}$, is a thermostabilizing mutation previously selected for using directed evolution for detergent stability (32) (Fig. S1). Homology models of α_{1A}-AR (Fig. 1) built on in inactive and active states of X-ray structures of β_2-AR show that three of these methionines were particularly interesting as conformational probes as they are located either within the adrenaline-binding site (Met-292$^{6.55}$), immediately adjacent to the highly conserved Ile-114$^{3.40}$ of the transmission switch (Met-115$^{3.41}$), or sitting above Tyr-125$^{3.51}$ of the DRY motif within the G protein-binding site (Met-203$^{5.57}$). These homology models of α_{1A}-AR suggest that each of these regions undergo significant local rearrangements between inactive to active conformations (Fig. 1).

α_{1A}-AR-A4 was expressed and labeled with [$^{13}C^{\epsilon}H_3$]methionine using an adapted *E. coli* methionine biosynthesis pathway inhibition protocol that we have previously used to generate [$^{13}C^{\epsilon}H_3$]methionine-labeled neurotensin receptor 1 (NTS_1) samples labeled with 96% incorporation efficiency (34, 35). Using this method α_{1A}-AR-A4 expressed well and could be purified, solubilized in *n*-dodecyl-β-D-maltopyranoside (DDM), with a yield of (0.5–1 mg/liter of culture). 40–60 μM samples of [$^{13}C^{\epsilon}H_3$]methionine-labeled α_{1A}-AR-A4 were subsequently used to record 2D ^{1}H-^{13}C SOFAST-heteronuclear multiple quantum coherence (HMQC) spectra in the apo state, and in the bound states for prazosin (full inverse agonist), WB-4101 (partial inverse agonist), phentolamine (partial inverse agonist), silodosin (or KMD-3213, neutral antagonist), oxymetazoline (partial agonist), and adrenaline (full agonist) (Fig. 2 and Fig. S2). Individual [$^{13}C^{\epsilon}H_3$]methionine resonances were assigned by expressing and analyzing α_{1A}-AR-A4 M80L, α_{1A}-AR-A4 M115I, α_{1A}-AR-A4 M203L, α_{1A}-AR-A4 M248I, and α_{1A}-AR-A4 M292I mutants in the same way. ^{1}H-^{13}C SOFAST-HMQC spectra enabled clear assignment of mutated methionines as the remaining five resonances in these spectra showed only small chemical shift differences in the presence of the mutation (Fig. S3). The [$^{13}C^{\epsilon}H_3$]methionine of the apo state of α_{1A}-AR-A4 showed clear single resonances for each methyl with no significant heterogeneity (Fig. 2), in contrast to many previously studied GPCRs (5, 8, 14, 20–22). Met-145$^{4.44}$ and Met-248^{ICL3} exhibited intense signals with ^{1}H and ^{13}C chemical shifts of the methyl group indicative of solvent-exposed, unrestrained methyl groups. Met-248^{ICL3}, located within ICL3 (Fig. 1*A*), showed strong signal intensity most likely due to the mobility of this loop and exposure to the bulk solvent. Met-145$^{4.44}$ is at the C-terminal intracellular end of TM4, predicted to be exposed on the surface of the helix (Fig. 1*A*) and thus also highly mobile. Met-80$^{2.58}$ was not unambiguously assigned (Fig. S3, *A* and *F*) as it either is significantly broadened and difficult to resolve in all receptor states or may overlap with Met-145$^{4.44}$ and under some conditions with Met-292$^{6.55}$ (Fig. S3*E*). The remaining methionines, Met-115$^{3.41}$, Met-203$^{5.57}$, and Met-292$^{6.55}$, were readily assigned (Fig. S3, *B*, *C*, *E*, *G*, *H*, and *J*) and exhibited resolved chemical shifts for the $^{13}C^{\epsilon}H_3$ that were sensitive to the bound ligand (Fig. 2, *B–D*).

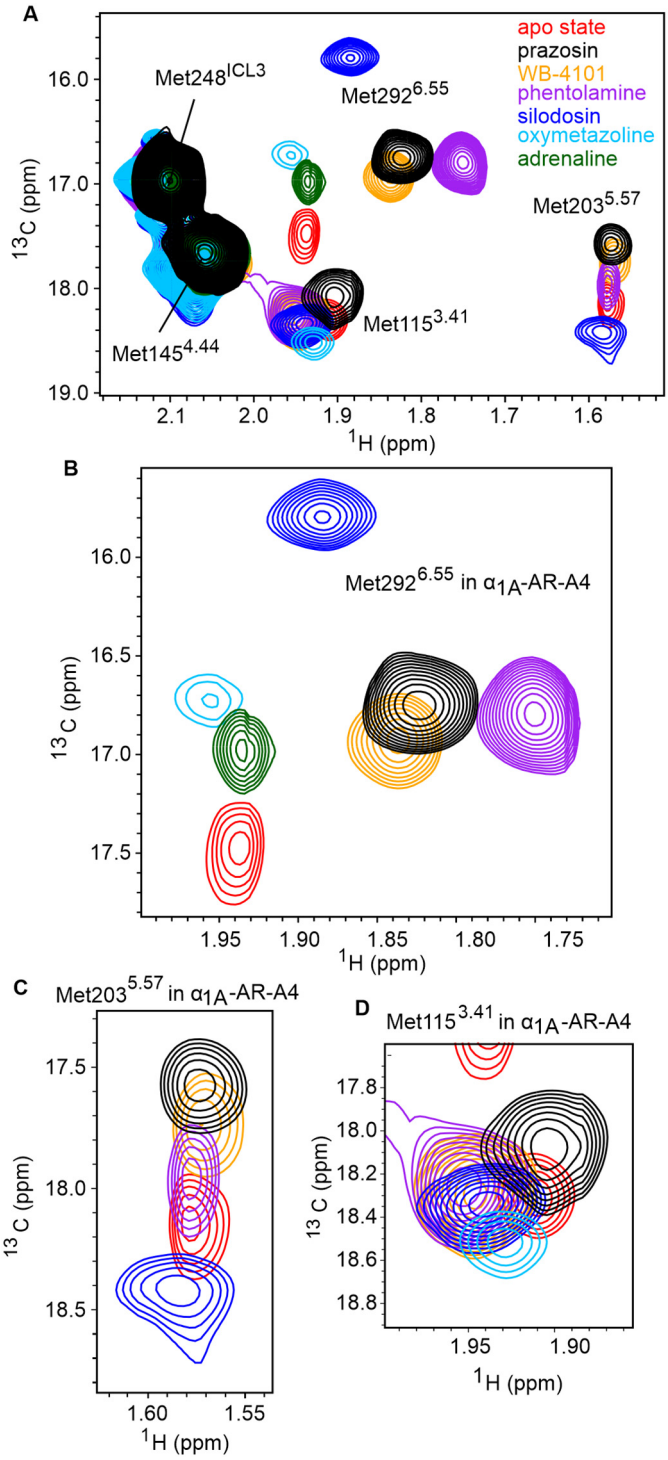

Figure 2. ^{1}H-^{13}C SOFAST-HMQC spectra of α_{1A}-AR-A4. *A*, overlay of 2D ^{1}H-^{13}C SOFAST-HMQC spectra for ([$^{13}C^{\epsilon}H_3$]Met-) α_{1A}-AR-A4 collected in the apo state (*red*) and bound to prazosin (*black*, inverse agonist), WB-4101 (*orange*, inverse agonist), phentolamine (*purple*, inverse agonist), silodosin (*blue*, neutral antagonist), oxymetazoline (*cyan*, partial agonist), and adrenaline (*green*, full agonist). *B*, close-up of the Met-292$^{6.55}$ resonance. *C*, close-up of the Met-203$^{5.57}$ resonance. *D*, close-up of the Met-115$^{3.41}$ resonance. Spectra were acquired on ~50 μM α_{1A}-AR-A4 dissolved in 0.02–0.1% DDM micelle, pH 7.5, and 25 °C.

Based on homology models, Met-292$^{6.55}$ projects into the orthosteric ligand-binding pocket (Fig. 1*A*) and mutational studies support a role for this residue in ligand binding (36). Thus, the $^{13}C^{\epsilon}H_3$ chemical shifts of Met-292$^{6.55}$ likely reflect a direct interaction with chemical groups of each ligand. Interestingly, the resonance intensities of Met-292$^{6.55}$ increased in the presence of antagonists and inverse agonists relative to the apo state (Fig. 2*B*), indicating that binding of these ligands reduces conformational dynamics in the orthosteric binding site. Met-115$^{3.41}$ and Met-203$^{5.57}$ are distant from the orthosteric site, but both the chemical shifts and line widths of their $^{13}C^{\epsilon}H_3$ groups were sensitive to ligand binding (Fig. 2, *C* and *D*), likely reflecting receptor conformational changes in the transmission switch and G protein-binding site, respectively (Fig. 1, *C* and *D*). The ^{1}H chemical shift of the methyl of Met-203$^{5.57}$ was shifted upfield from typical small-peptide positions (2.1 ppm) to 1.58 ppm in agreement with our models, which predict ring-current induced effects from Tyr-125$^{3.51}$ of the DRY motif (Fig. S4). Met-203$^{5.57}$ therefore serves as a probe of conformational change within this region. Indeed, the resonances of the $^{13}C^{\epsilon}H_3$ of Met-203$^{5.57}$ exhibited a significant linear chemical shift change depending on which ligand was bound, demonstrating that allosteric coupling between the ligand-binding site and the G protein-binding site is retained in the inactive α_{1A}-AR-A4 in solution. Such a linear chemical shift change is also expected for ligands modulating the receptor state via conformational selection. We postulate that the Met-203$^{5.57}$ signal reflects the average, equilibrium signal, between inactive and active states undergoing fast exchange. Inverse agonists preferentially bound to inactive states, shifting the Met-203$^{5.57}$ equilibrium to an upfield position (inactive state) compared with the apo state receptor, which can sample active-like states to a certain degree.

We were interested to see if an opposite trend could be observed for receptor agonists, which we hypothesized would shift the position of the Met-203$^{5.57}$ resonance downfield. For α_{1A}-AR-A4, however, the binding of the full agonist adrenaline to α_{1A}-AR-A4 resulted in complete line broadening of the Met-115$^{3.41}$ and Met-203$^{5.57}$ resonances despite the promotion of a distinct chemical shift for Met292$^{6.55}$ in the binding site. Binding of the partial agonist oxymetazoline resulted in substantial broadening of Met-203$^{5.57}$ and Met-292$^{6.55}$, but not Met-115$^{3.41}$. The loss of these chemical shifts upon agonist binding was likely due to the significantly weaker agonist affinities at α_{1A}-AR-A4 compared with unmutated, WT α_{1A}-AR, as a result of the F312L-stabilizing mutation (32). Thus, NMR experiments were repeated on α_{1A}-AR-A4 (L312F), for which agonist affinities were largely restored to that of WT α_{1A}-AR (Fig. S5 and Table S1) (32).

Agonist-induced chemical shifts of Met-115$^{3.41}$ and Met-203$^{5.57}$ resonances

Despite the reduced thermostability of α_{1A}-AR-A4 (L312F) (32), we were able to [$^{13}C^{\epsilon}H_3$]methionine label and record ^{1}H-^{13}C SOFAST-HMQC spectra for this receptor in the apo state and bound to adrenaline (full agonist), phenylephrine (full agonist), A-61603 (full agonist), and oxymetazoline (partial agonist) in addition to the inverse agonists and neutral antagonists tested on α_{1A}-AR-A4 (Fig. 3*A*). Overall, the ^{1}H-^{13}C SOFAST-HMQC spectra of the apo, antagonist, and inverse agonist-bound states of α_{1A}-AR-A4 (L312F) were similar to those of α_{1A}-AR-A4. Again, single resonances for the [$^{13}C^{\epsilon}H_3$]methionine groups of α_{1A}-AR-A4 (L312F) were observed for all ligands. The chemical shifts of Met-292$^{6.55}$ induced by each ligand in α_{1A}-AR-A4 (L312F) were slightly different to those of α_{1A}-AR-A4, most likely due to orthosteric binding site changes after the L312F reversion. Inverse agonist binding increased the intensity of the Met-292$^{6.55}$ resonance in α_{1A}-AR-A4 (L312F), as was seen with α_{1A}-AR-A4; whereas the neutral antagonist silodosin significantly decreased the peak intensity and the partial agonist oxymetazoline and full agonist A-61603 highly broadened the resonance of Met-292$^{6.55}$ in α_{1A}-AR-A4 (L312F) (Fig. S6).

The recovered agonist affinity for α_{1A}-AR-A4 (L312F) allowed the measurement of ^{1}H-^{13}C SOFAST-HMQC spectra where we were confident of full receptor-agonist saturation. Binding of the full agonist adrenaline to α_{1A}-AR-A4 (L312F) produced a similar Met-292$^{6.55}$ chemical shift to that seen with α_{1A}-AR-A4 (Fig. 3*A*), and also weak peaks were now observed for Met-115$^{3.41}$ and Met-203$^{5.57}$ (Fig. 3, *B* and *C*), which were completely broadened in adrenaline-bound α_{1A}-AR-A4. Importantly, the binding of all agonists, adrenaline, phenylephrine, and A-61603 to α_{1A}-AR-A4 (L312F) induced distinct chemical shift and line broadening changes to Met-115$^{3.41}$ and Met-203$^{5.57}$ compared with neutral antagonists and inverse agonists (Fig. 3, *B* and *C*). The agonist-induced Met-115$^{3.41}$ resonances cluster together as potentially indicative of an active transmission switch conformation (Fig. 3*B*). Binding of the partial agonist oxymetazoline induced a chemical shift of Met-115$^{3.41}$ falling between the inverse agonist and full agonist clusters, consistent with partial agonists promoting a weaker shift in the inactive-active transmission switch state equilibrium. The linear change in the Met-203$^{5.57}$ chemical shift position upon inverse agonist binding seen with α_{1A}-AR-A4 was retained in α_{1A}-AR-A4 (L312F), but as hypothesized, agonist binding promoted opposite, downfield resonance shifts in the ^{13}C dimension along the same vector (Fig. 3*C*). This change in [$^{13}C^{\epsilon}H_3$]methionine chemical shift in the ^{13}C dimension reflects a change in the χ3 dihedral angle. The ^{13}C chemical shift dependence of this angle is about 19 ppm for trans and 16 ppm for ±gauche (37). For the apo and antagonist states the chemical shift of 18.25 to 18.5 ppm suggests a trend toward trans, whereas in the full-inverse agonist state the resonance shifts up-field to 17.7 ppm, indicative of an averaging between gauche and trans. Consistent with our homology models (Fig. S4) for full agonist a further downfield shift between 19 and 19.25 ppm infers an increase in the trans conformer. Interestingly, the partial agonist oxymetazoline induced a small upfield $^{13}C^{\epsilon}$ shift of Met-203$^{5.57}$, similar to the inverse agonist phentolamine. The fact that full agonists induced Met-203$^{5.57}$ chemical shifts to move in the opposite direction to inverse agonists suggests an equilibrium shift away from inactive to active conformational states of the DRY motif. Furthermore, the resonance intensities of both Met-115$^{3.41}$ and Met-203$^{5.57}$ in α_{1A}-AR-A4 (L312F), relative to the ligand-insensitive Met-145$^{4.44}$ resonance, were weakened upon agonist binding compared with the

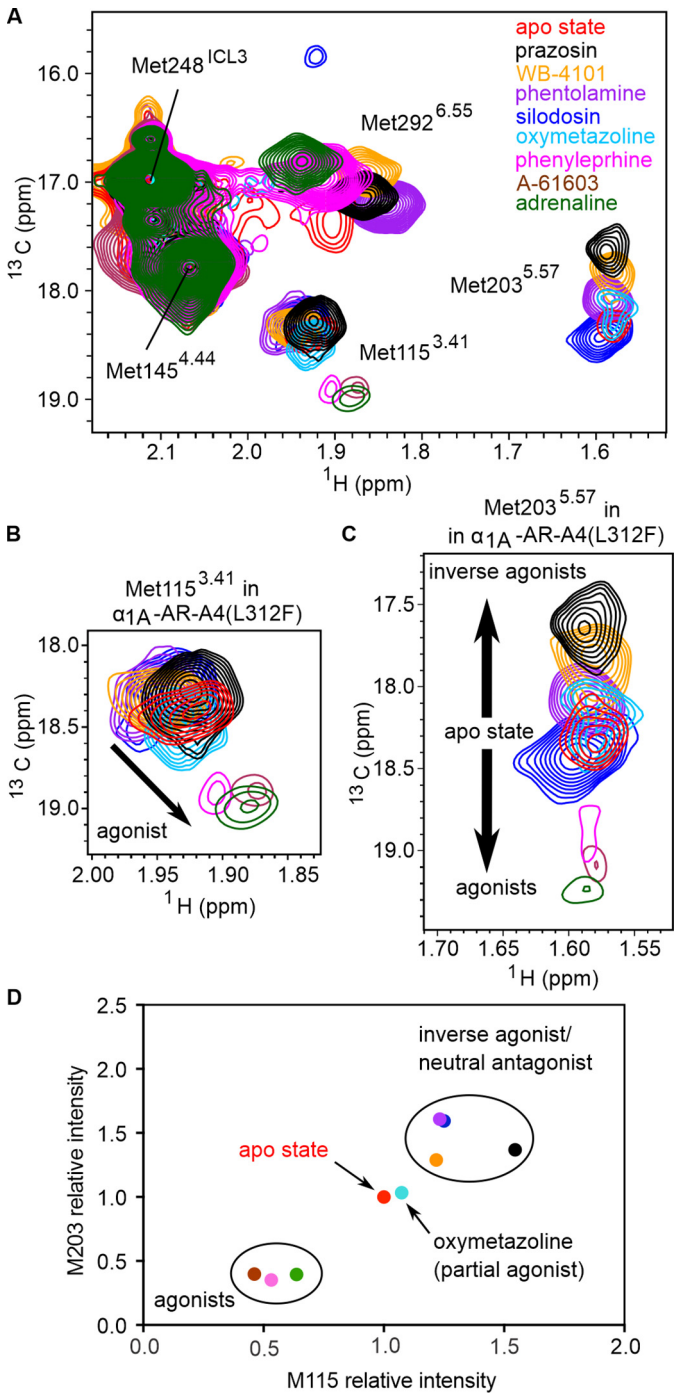

Figure 3. Ligand efficacy-dependent chemical shifts of Met-115$^{3.41}$ and Met-203$^{5.57}$ resonances. *A*, overlay of 2D ^{1}H-^{13}C SOFAST-HMQC spectra for ([$^{13}C^{\epsilon}H_3$]Met-) α_{1A}-AR-A4 (L312F) in the apo state (*red*) and bound to ligands: prazosin (*black*, inverse agonist), WB-4101 (*orange*, inverse agonist), phentolamine (*purple*, inverse agonist), silodosin (*blue*, neutral antagonist), oxymetazoline (*cyan*, partial agonist), phenylephrine (*magenta*, full agonist), A-61603 (*maroon*, full agonist), and adrenaline (*green*, full agonist). *B*, close-up of the Met-115$^{3.41}$ resonance in α_{1A}-AR-A4 (L312F). *C*, close-up of the Met-203$^{5.57}$ resonance in α_{1A}-AR-A4 (L312F). The spectra for adrenaline, A-61603, and phenylephrine are plotted at a level 1.8-times lower than the main figure. *D*, normalized peak intensities of Met-115$^{3.41}$ and Met-203$^{5.57}$ of α_{1A}-AR-A4 (L312F) show differences between agonists, antagonists, and partial agonists. Ligands are colored as listed above. Spectra were acquired on ~50 μM α_{1A}-AR-A4 (L312F) dissolved in 0.02–0.1% DDM micelle, pH 7.5, and 25 °C.

intensity increases seen with antagonists and inverse agonists (Fig. 3*D*). The intensities of Met-115$^{3.41}$ and Met-203$^{5.57}$ upon binding of the partial agonist oxymetazoline fell between the antagonist- and agonist-induced intensities. The behavior of the $^{13}C^{\epsilon}H_3$ of Met-115$^{3.41}$ and Met-203$^{5.57}$ is consistent with the current concept that agonists increase conformational heterogeneity in GPCRs, where agonists increase microsecond timescale transitions to active receptor states, to increase the probability of engaging and activating effector proteins (5, 8, 10, 14, 15, 23).

Chemical shift changes of Met-203$^{5.57}$ correlate with ligand efficacy

In mammalian cells, α_{1A}-AR exhibits basal activity in the absence of bound ligands (38). Such basal activity is unaffected by the binding of neutral antagonists but is reduced by the binding of inverse agonists to the receptor. In the case of α_{1A}-AR, by probing the ability of various antagonists to reduce the signaling of a constitutively active receptor mutant, the rank order of inverse agonist efficacies has been found to be: prazosin (strongest); WB-4101, phentolamine (weakest), and silodosin being a neutral antagonist (38). To understand how the NMR signals of Met-203$^{5.57}$ in α_{1A}-AR-A4 (L312F) relate to receptor conformational equilibria, the changes to the chemical shifts for the $^{13}C^{\epsilon}H_3$ of Met-203$^{5.57}$ were plotted against the previously published relative efficacy values for the inverse agonists, revealing a strong linear correlation ($R^2 = 0.99$, Fig. 4*A*). To test if this correlation is retained when probing inverse agonism at the WT α_{1A}-AR, we determined the relative inverse agonist efficacies of these ligands using a NanoBiT split luciferase assay (39). In this assay the 18-kDa Large BiT (LgBiT) fragment was fused to the N terminus of Gα_q and the 1.3-kDa Small BiT (SmBiT) was fused to the N terminus of Gγ_2. When co-expressed with Gβ_1, the formation of a Gα_q(LgBiT)-Gβ_1-Gγ_2(SmBiT) heterotrimer results in bright luminescence. GPCR-induced stimulation of this G protein complex causes dissociation of the heterotrimer and thus reduction in luminescence output, whereas inhibition of basal GPCR activation would be predicted to increase luminescence output. COS-7 African green monkey kidney cells stably expressing WT α_{1A}-AR were transfected with Gα_q(LgBiT), Gβ_1, and Gγ_2(SmBiT) encoding expression plasmids, incubated with luminescence substrate, and then treated with various α_{1A}-AR ligands, while monitoring cellular luminescence. A-61603 induced α_{1A}-AR activation led to heterotrimer dissociation of the Gα_q(LgBiT)-Gβ_1-Gγ_2(SmBiT) complex and thus a reduction in luminescence output (Fig. 4*B*). Inverse agonists on the other hand reduced basal activation of α_{1A}-AR, maintaining the Gα_q(LgBiT)-Gβ_1-Gγ_2(SmBiT) complex leading to increased luminescence output from the cells (Fig. 4*B*). The specificity of these responses was probed by conducting the same experiments on COS-7 cells not expressing α_{1A}-AR (Fig. S7, *A–C*). The observed changes in luminescence after α_1-AR ligand treatments were specific to α_{1A}-AR expressing cells except for WB-4101, which induced a short (5 min) increase in luminescence in the control cells (Fig. S7*A*). To exclude this nonspecific effect the net luminescence change for each sample group was calculated as the area under the luminescence curves between

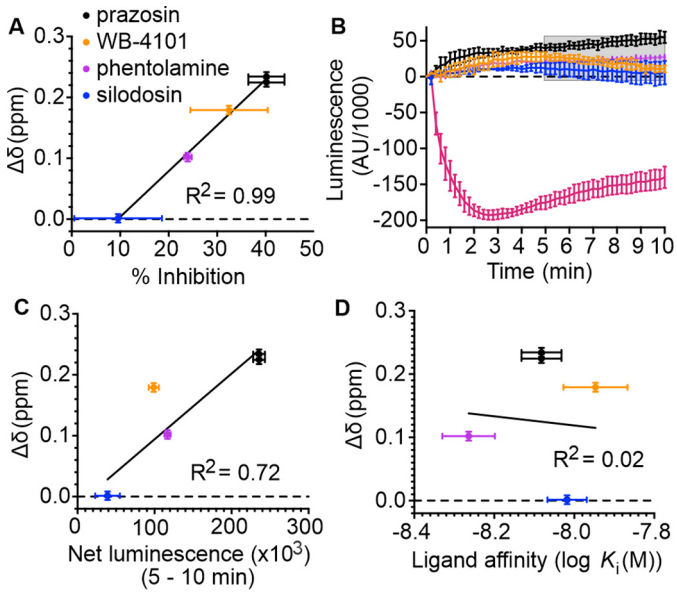

Figure 4. Correlation between the chemical shift positions of the $^{13}C^{\epsilon}H_3$ in Met-203$^{5.57}$ and inverse agonists efficacy. *A,* linear regression analysis of the average chemical shift differences (Δδ) for the $^{13}C^{\epsilon}H_3$ of Met-203$^{5.57}$ in α_{1A}-AR-A4 (L312F) when bound to prazosin (*black circles*), WB-4101 (*orange circles*), and phentolamine (*purple circles*) compared with silodosin (*blue circles*) and the published efficacy of each ligand in reducing the signaling of a constitutively active mutant of α_{1A}-AR (38). Published data were extracted using WebPlotDigitizer (RRID: SCR_013996). Testing the resultant equation against the null hypothesis of a slope of zero resulted in a *p* value of <0.0001. *B,* NanoBit G protein activity assay demonstrating inverse agonism of prazosin, WB-4101, phentolamine, and silodosin at WT α_{1A}-AR–expressing COS-7 cells. Each of these inverse agonist experiments were repeated in three independent biological replicate experiments, with the mean ± S.E. of the resultant luminescence plotted for each time point. To demonstrate the response from an agonist, A-61603 treatment was performed in two independent biological replicate experiments. Each biological replicate comprised three technical replicates measured in parallel. The *gray shaded* region indicates where the area under each biological replicate curve was calculated for *C*. *C,* linear regression analysis of the average chemical shift differences (Δδ) for the $^{13}C^{\epsilon}H_3$ of Met-203$^{5.57}$ in α_{1A}-AR-A4 (L312F) and the increase in luminescence seen in the NanoBit assay for each inverse agonist and neutral antagonist. Ligands are colored as listed above and the *p* value testing against a slope of 0 was 0.011. *D,* linear regression analysis of the average chemical shift differences (Δδ) for the $^{13}C^{\epsilon}H_3$ of Met-203$^{5.57}$ in α_{1A}-AR-A4 (L312F) and the affinities of each inverse agonist and neutral antagonist. Ligands are colored as listed above and the *p* value testing against a slope of 0 was 0.89. In *A*, *C*, and *D*, Δδ is plotted for two independent titrations of prazosin and silodosin, and single experiments for WB-4101 and phentolamine. Average chemical shift differences (Δδ) were normalized using the equation $\Delta\delta = [(\Delta\delta_{1H})^2 + (\Delta\delta_{13C}/3.5)^2]^{0.5}$ and error was calculated by the formula $|[\Delta\delta_{1H} \times R_{1H} + \Delta\delta_{13C} \times R_{13C}/(3.5)^2]|/\Delta\delta$, where R_{1H} and R_{13C} are the digital resolutions in ppm in the ^{1}H and ^{13}C dimensions, respectively (5).

5 and 10 min after ligand addition. A strong linear correlation was found between the chemical shift changes for the $^{13}C^{\epsilon}H_3$ of Met-203$^{5.57}$ in α_{1A}-AR-A4 (L312F) and the net luminescence increase generated by each inverse agonist over the 5-min period in the WT α_{1A}-AR-expressing cells ($R^2 = 0.72$, Fig. 4*C*). Importantly, the Met-203$^{5.57}$ chemical shift positions of α_{1A}-AR-A4 (L312F) did not correlate with the affinity of these antagonists for α_{1A}-AR (Fig. 4*D*), demonstrating that the differences in chemical shift were not due to varying receptor occupancy. Furthermore, no correlation was seen between the [$^{13}C^{\epsilon}H_3$]Met-203$^{5.57}$ chemical shift changes of α_{1A}-AR-A4 (L312F) and the net luminescence changes in COS-7 cells not expressing WT α_{1A}-AR (Fig. S7*B*). Critically, the correlation between chemical shift changes of [$^{13}C^{\epsilon}H_3$]Met-203$^{5.57}$ in α_{1A}-AR-A4 (L312F) and WT α_{1A}-AR–specific luminescence increases in the NanoBiT assay remained when the analysis window was extended to include the full 10 min after ligand addition (Fig. S7*D*).

Improving signaling competency in α_{1A}-AR-A4

When expressed in COS-7 cells, α_{1A}-AR-A4 is incapable of stimulating cellular increases in inositol phosphate 1 (IP_1) in response to adrenaline binding, or activation of a cAMP response element (CRE) reporter gene after treatment with another α_1-AR agonist, phenylephrine (32). To ensure biological relevance of our NMR studies we thus sought α_{1A}-AR-A4 back-mutants that were able to stimulate canonical signaling pathways in mammalian cells upon agonist treatment. Seven thermostabilizing mutations within the TMD of α_{1A}-AR-A4 were back-mutated (Y67N, M80L, A127G, F151W, K322N, L327P, and Y329S) as single changes or in combinations, and screened for phenylephrine- and oxymetazoline-induced signaling with an IP_1 assay in transfected COS-7 cells (Fig. S8*A*). Although the back-mutant, α_{1A}-AR-A4 (Y67N, M80L, K322N, L327P, and Y329S) was able to facilitate significant oxymetazoline-induced cellular accumulation of IP_1 compared with α_{1A}-AR-A4 and WT α_{1A}-AR (Fig. S8*A*) it expressed poorly in bacteria. The back-mutant α_{1A}-AR-A4 (Y67N, K322N), termed α_{1A}-AR-A4–active, however, was able to stimulate IP_1 accumulation in response to both phenylephrine and oxymetazoline treatment (Fig. S8*A*) and it expressed well in bacteria. Importantly, α_{1A}-AR-A4 contains the N322K-stabilizing mutation in the NP*XXY* switch(25), which is hypothesized to form a stabilizing salt bridge with Asp-72$^{2.50}$ to lock the NP*XXY* switch in an inactive and stable state. We thus expected that reversion of this mutation (K322N) would restore the function of the NP*XXY* switch and the signaling activity of α_{1A}-AR-A4. Interestingly, the Y67N mutation was required on top of K322N to restore signaling activity in α_{1A}-AR-A4–active. Asn-67$^{2.45}$ is distant from the NP*XXY* switch and its importance is not clear.

Using an intracellular calcium mobilization assay, α_{1A}-AR-A4–active was able to be activated by the full agonists adrenaline and A-61603, as well as the partial agonists oxymetazoline and PF-3774076 (Fig. S8, *B–E*). The affinity of QAPB for α_{1A}-AR-A4–active was retained upon purification of the receptor in DDM (Fig. S9*A*). Competition binding assays revealed, however, that the affinities of agonists for α_{1A}-AR-A4–active (Fig. S9*B* and Table S1) were weaker than WT α_{1A}-AR due to the F312L stabilizing mutation, but stronger than at α_{1A}-AR-A4 (32). When purified in DDM α_{1A}-AR-A4–active was significantly less stable than α_{1A}-AR-A4 (Fig. S9*C*) and thus back-mutation of F312L to recover agonist potency was not pursued as it was deemed unlikely that the resultant receptor would be stable enough for NMR experiments.

α_{1A}-AR-A4–active was labeled with [$^{13}C^{\epsilon}H_3$]methionine and 2D ^{1}H-^{13}C SOFAST-HMQC spectra were acquired as above (Fig. 5, *A* and *D*). Overall the ligand-perturbed chemical shifts of the [$^{13}C^{\epsilon}H_3$]methionine resonances in α_{1A}-AR-A4–active were similar to those in α_{1A}-AR-A4 and α_{1A}-AR-A4 (L312F), except for several key differences with the Met-115$^{3.41}$ and Met-203$^{5.57}$ resonances. We acquired spectra of four independent preparations of apo α_{1A}-AR-A4–active (four biologi-

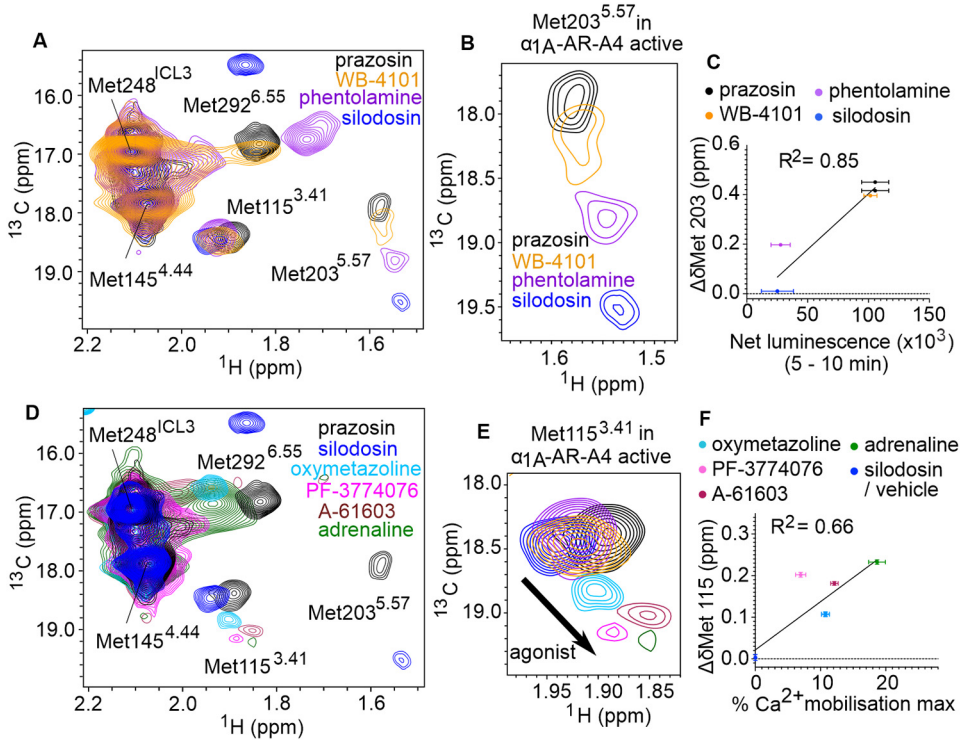

Figure 5. ^{1}H-^{13}C SOFAST-HMQC spectra of α_{1A}-AR-A4–active. *A,* Overlay of 2D ^{1}H-^{13}C SOFAST-HMQC spectra of ([$^{13}C^{\epsilon}H_3$]Met-) α_{1A}-AR-A4–active bound to prazosin (*black*, inverse agonist), WB-4101 (*orange*, inverse agonist), phentolamine (*purple*, inverse agonist), and silodosin (*blue*, neutral antagonist). *B,* close-up of the Met-203$^{5.57}$ resonance. *C,* linear regression analysis of the average chemical shift differences (Δδ) for the $^{13}C^{\epsilon}H_3$ of Met-203$^{5.57}$ in α_{1A}-AR-A4–active when bound to prazosin (*black circles*), WB-4101 (*orange circles*), and phentolamine (*purple circles*) compared with silodosin (*blue circles*) and the increase in luminescence seen in the NanoBit assay with α_{1A}-AR-A4–active expressing COS-7 cells treated with the same antagonist (from Fig. S11*A*). Testing the resultant equation against the null hypothesis of a slope of zero resulted in a *p* value of 0.0041. *D,* overlay of 2D ^{1}H-^{13}C SOFAST-HMQC spectra of ([$^{13}C^{\epsilon}H_3$]Met-) α_{1A}-AR-A4–active bound to prazosin (*black*, inverse agonist), silodosin (*blue*, neutral antagonist), oxymetazoline (*cyan*, partial agonist), PF-3774076 (*magenta*, partial agonist), A-61603 (*maroon*, full agonist), and adrenaline (*green*, full agonist). *E,* close-up of the Met-115$^{3.41}$ resonance. *F,* linear regression analysis of the average chemical shift differences (Δδ) for the $^{13}C^{\epsilon}H_3$ of Met-115$^{3.41}$ in α_{1A}-AR-A4–active when bound to oxymetazoline (*cyan circles*), PF-3774076 (*pink circles*), A-61603 (*dark red circles*), adrenaline (*green circles*), and silodosin (*blue circles*) and the efficacy of each agonist in triggering Ca^{2+} mobilization in α_{1A}-AR-A4–active expressing COS-7 cells (from Fig. S8, *B–E*). Testing the resultant equation against the null hypothesis of a slope of zero resulted in a *p* value of 0.0154. *C* and *F,* Δδ are plotted for two independent titrations of prazosin, silodosin, and oxymetazoline, and single experiments for other ligands. In *A*, *B*, *D*, and *E*, spectra were acquired on ~50 μM α_{1A}-AR-A4–active dissolved in 0.02–0.1% DDM micelle, pH 7.5, and 25 °C. Average chemical shift differences (Δδ) were normalized using the equation $\Delta\delta = [(\Delta\delta_{1H})^2 + (\Delta\delta_{13C}/3.5)^2]^{0.5}$ and errors were calculated by the formula $|[\Delta\delta_{1H} \times R_{1H} + \Delta\delta_{13C} \times R_{13C}/(3.5)^2]|/\Delta\delta$, where R_{1H} and R_{13C} are the digital resolutions in ppm in the ^{1}H and ^{13}C dimensions respectively (5).

cal replicates) and found that in the absence of bound ligand the data were not easily reproduced (Fig. S10*A*). The well-resolved Met-203$^{5.57}$ varied between an intense peak, two peaks of similar intensity, or a peak of weak intensity. Met-115$^{3.41}$ persisted as a split peak, although the two components varied in intensity. Importantly, in the presence of the most potent inverse agonist, prazosin, the resonances of Met-115$^{3.41}$ and Met-203$^{5.57}$ were single peaks, and regardless of sample preparation, exhibited the same chemical shifts. The [$^{13}C^{\epsilon}H_3$]Met-115$^{3.41}$ resonance, as perturbed by prazosin, aligned approximately with the upfield component of the resonance for apo α_{1A}-AR-A4–active (Fig. S10*B*). In contrast, upon titration with the neutral antagonist, silodosin, the peaks of Met-115$^{3.41}$ also collapsed to a single resonance with identical chemical shifts, but now aligned best with the downfield component of apo α_{1A}-AR-A4–active (Fig. S10*B*). For the two partial inverse agonists, WB-4101 and phentolamine, the $^{13}C^{\epsilon}H_3$ resonance of Met-115$^{3.41}$ was a single resonance, positioned midway between the "prazosin" (upfield) and "silodosin" (downfield) peaks (Fig. 5*E*). These trends for ligand efficacy were present in α_{1A}-AR-A4 and α_{1A}-AR-A4 (L312F), but were not as distinct as now observed for α_{1A}-AR-A4–active, and notably the apo states for α_{1A}-AR-A4 and α_{1A}-AR-A4 (L312F) did not show two discrete peaks for Met-115$^{3.41}$. Such apo state sample-to-sample heterogeneity may suggest the presence of misfolded contaminants, but upon the addition of prazosin or silodosin each of these samples gave identical spectra (Fig. S10*A*), supporting the binding competency of the α_{1A}-AR-A4–active samples. The diversity of apo state spectra likely reflects diversity of conformational states of similar free energy. The addition of agonist again resulted in a single resonance for [$^{13}C^{\epsilon}H_3$]Met-115$^{3.41}$ that shifts upfield in ^{1}H and downfield in ^{13}C (Fig. 5*E*). The trend in shifts of these resonances, however, suggests they follow in a linear manner evolving from the downfield (basal) signal of the apo state and reflects the selection of the active-like state.

A major difference between the spectra of α_{1A}-AR-A4 and α_{1A}-AR-A4–active, however, was significantly increased line broadening of the Met-203$^{5.57}$ signal of α_{1A}-AR-A4–active in the apo state (Fig. S10*A*) and when bound to antagonists (Fig. 5*B*). This broadening suggests that the DRY motif near the G protein-binding site of α_{1A}-AR-A4–active is more dynamic compared with α_{1A}-AR-A4, consistent with a receptor that more readily transitions between inactive and active-receptor states. Importantly, similar to α_{1A}-AR-A4 and α_{1A}-AR-A4

(L312F) variants, the $^{13}C^{\epsilon}H_3$ of Met-203$^{5.57}$ shows an efficacy-dependent linear $^{13}C^{\epsilon}H_3$ chemical shift change in the presence of inverse agonist and neutral antagonist, trending to an upfield ^{13}C position ($\chi 3$ of $\pm$gauche) for the more potent inverse agonist (Fig. 5, *A* and *B*). Unexpectedly, the addition of silodosin (neutral antagonist) resulted in a significant ^{13}C downfield shift to near 19.5 ppm consistent with a trans $\chi 3$ angle for Met-203$^{5.57}$. Furthermore, similar to α_{1A}-AR-A4, the Met-203$^{5.57}$ $^{13}C^{\epsilon}H_3$ resonance of α_{1A}-AR-A4–active was near completely broadened in the presence of agonists.

NanoBiT G protein activity assays were performed on COS-7 cells expressing α_{1A}-AR-A4–active to determine relative inverse agonist efficacies. The inverse agonists reduced basal G_q activity in α_{1A}-AR-A4–active in a similar way as WT α_{1A}-AR expressing cells (Fig. 4*A* and Fig. S11*A*). The net luminescence change induced by each inverse agonist at α_{1A}-AR-A4–active expressing cells correlated well, in a linear fashion, with the $^{13}C^{\epsilon}H_3$ chemical shift changes of Met-203$^{5.57}$ that each ligand induced at purified α_{1A}-AR-A4–active, when analyzed over two separate time periods (Fig. 5*C* and Fig. S11*B*). Interestingly, the agonist-induced chemical shift changes of [$^{13}C^{\epsilon}H_3$]Met-115$^{3.41}$ showed a linear correlation with the efficacy of each agonist in Ca^{2+} mobilization assays on α_{1A}-AR-A4–active expressing COS-7 cells (Fig. 5*F*) although the partial agonist PF-3774076 was a notable outlier. Overall, these cell-based assays with the ligand efficacy-correlated chemical shift changes of Met-115$^{3.41}$ and Met-203$^{5.57}$ clearly demonstrate that a conformational selection mechanism underlies receptor function in cells.

Discussion

Recent spectroscopic studies have demonstrated that different classes of GPCR ligands distinctly alter the population of receptor states within the GPCR conformational equilibrium (23). GPCR conformational changes are driven by defined structural changes in the microswitches (24–26, 28) (Fig. 1) and, thus, how particular ligands affect the GPCR microswitch states likely underlies their pharmacological output as inverse, partial, full, or biased agonists. Observing these effects, however, remains challenging. α_{1A}-AR was one of the first GPCRs to be cloned and pharmacologically characterized (40) and is clinically targeted with agonists as nasal decongestants and antagonists for hypertension and BPH. Despite the importance of this receptor there are currently no three-dimensional structures of α_{1A}-AR, reflecting the inherent instability of this protein. Here, we demonstrate that prototypical ligands modulate the conformational equilibrium, as measured at the microswitches, of α_{1A}-AR in defined and predictable ways by [$^{13}C^{\epsilon}H_3$]methionine labeling α_{1A}-AR variants and monitoring the ^1H and ^{13}C chemical shifts of these methyl resonances in the presence of ligands of different efficacy.

It is well-accepted that the NMR signals of methionine methyl groups are sensitive to the local environment and the conformation of the methionine side chain (5, 8). Many of the conclusions made in this study rely on Met-115$^{3.41}$, a probe for the conformation of the transmission switch, and Met-203$^{5.57}$ as a probe of the DRY motif that signifies intracellular TMD rearrangements for G-protein binding. In our model of α_{1A}-AR, Met-203$^{5.57}$ sits over Tyr-125$^{3.51}$ of the DRY motif but is distant from Arg-124$^{3.50}$, which is expected to undergo significant rotameric changes within this motif (2) (Fig. 1*D*). Met-115$^{3.41}$ is sequential to the Ile-114$^{3.40}$ in TM3 but it points away and is distant to the transmission switch residue Phe-281$^{6.44}$ located on TM6, which is expected to undergo significant rotameric changes (Fig. 1*C*). Although, in the thermostabilized inactive α_{1A}-AR-A4 mutant the residues of the transmission switch and DRY motif are retained, the asparagine of a third microswitch, the NP*XX*Y motif, is mutated to lysine, which likely forms a salt bridge with Asp-72$^{2.50}$ to lock this switch in an inactive state. The transmission switch and NP*XX*Y motif are proximal to each other and therefore Met-115$^{3.41}$, whereas distant to NP*XX*Y, is likely to be sensitive to conformational changes involving both switches. In the reported active-state GPCR structures, three conserved residues (Arg$^{3.50}$ of the DRY motif, Tyr$^{7.53}$ of the NP*XX*Y motif, and Tyr$^{5.58}$) adopt near identical positions and connect these microswitches through water-mediated hydrogen bonds (1, 2). Furthermore, in our model of active α_{1A}-AR, which is based on structures of β_2-AR, Arg-124$^{3.50}$ of the DRY motif is in contact with Tyr-326$^{7.53}$ of the NP*XX*Y motif (Fig. 1*D*).

In our NMR experiments for all ligands the $^{13}C^{\epsilon}H_3$ group of both Met-115$^{3.41}$ and Met-203$^{5.57}$ show significant directional chemical shift and line width changes that are correlated with ligand efficacy, not affinity. As a distinct peak is observed for the addition of each ligand the chemical shift likely reflects an average population exchanging on a fast to intermediate timescale. The chemical shift differences, however, reflect a shift in the equilibrium, and specifically for the $^{13}C^{\epsilon}H_3$ of Met-203$^{5.57}$, from a $\chi 3$ of a gauche-trans average (inverse agonist) toward a trans (agonist) average (Fig. 6*A*). An NMR study using ^{15}N-labeled, thermostabilized β_1-AR observed substantial ligand efficacy-correlated backbone chemical shift changes for Val-226$^{5.57}$, which is in the same position as Met-203$^{5.57}$ in α_{1A}-AR (13). The authors speculated that these changes were caused by TM5 bending toward the active receptor state (13), an idea that may also apply to α_{1A}-AR and other GPCRs. Here, the linear chemical shift changes of Met-203$^{5.57}$, and to a lesser degree Met-115$^{3.41}$, in response to ligands of different efficacy is strong evidence that agonists activate α_{1A}-AR via a conformational selection mechanism. The line broadening of Met-115$^{3.41}$ and Met-203$^{5.57}$ upon agonist binding supports an efficacy-driven shift in dynamics, and thereby the equilibrium of conformational states, communicated allosterically by the microswitches and sensed by these methionine residues (Fig. 6).

For our signaling incompetent receptors, α_{1A}-AR-A4 and α_{1A}-AR-A4 (L312F), the NP*XX*Y microswitch has been mutated (N322K) in a way that would bias the NP*XX*Y switch toward inactive states (Lys-322–Asp-72 salt bridge). A consequence of this mutation is that for α_{1A}-AR-A4 (L312F) the DRY motif probe, Met-203$^{5.57}$, gives relatively intense chemical shifts in the apo and antagonist-bound states (conformational equilibrium biased toward inactive states) (Fig. 6*B*). On restoration of the NP*XX*Y microswitch in α_{1A}-AR-A4–active, however, the Met-203$^{5.57}$ chemical shifts broaden and shift toward the agonist-bound position (as defined for α_{1A}-AR-A4 (L312F)), even with neutral antagonist bound. Therefore,

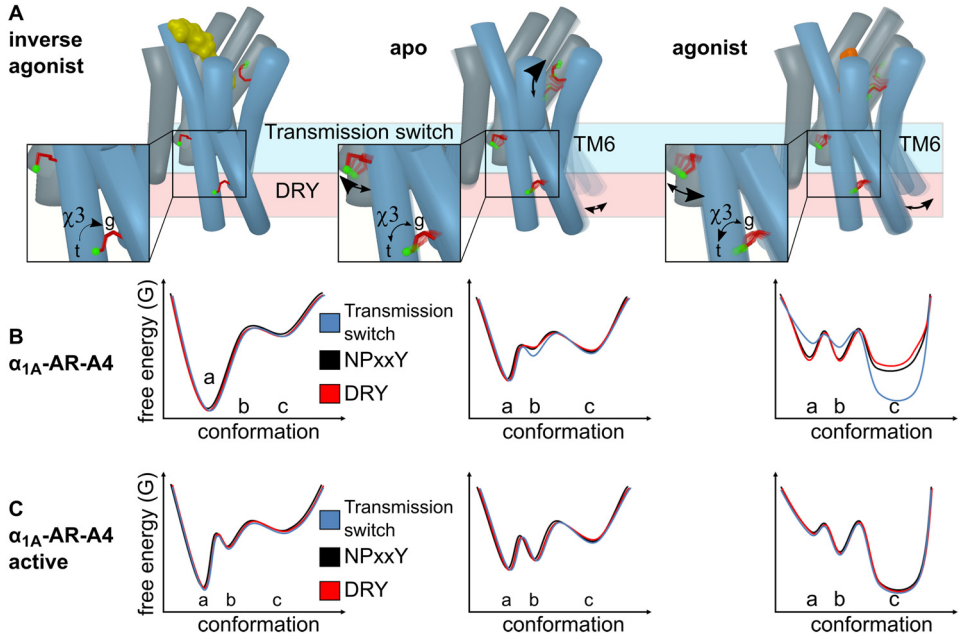

Figure 6. How ligands modulate the conformational landscape of the α_{1A}-AR microswitches. *A*, cartoon representations of α_{1A}-AR in the inverse agonist-bound, apo, and agonist-bound states. The three probe methionines, Met-292$^{6.55}$ (*binding site*), Met-115$^{3.41}$ (*transmission switch*), and Met-203$^{5.57}$ (DRY microswitch) are highlighted with *red sticks* and the labeled methyl group in *green*. The *arrows* labeled χ3 illustrate the ligand-induced changes to the equilibrium between the trans (*t*) and gauche (*g*) χ3 dihedral angle of Met-203$^{5.57}$. *Other arrows* indicate how different ligands alter the conformation equilibria of Met-292$^{6.55}$, Met-115$^{3.41}$, and TM6. Hypothetical free energy landscape diagrams of the three microswitches in (*b*) the inactive α_{1A}-AR-A4 receptor compared with (*C*) α_{1A}-AR-A4–active. (*a*) indicates the proposed inactive states, (*b*) represents basal states, and (*c*) represents active states of the microswitches.

restoring the NP*XX*Y microswitch enables the DRY motif of α_{1A}-AR-A4–active to more readily sample active-like states. The full trans (19.5 ppm in ^{13}C) populated by silodosin indicates that we may observe the full-active state, although previous studies showed that the full-active state is only populated in the presence of both agonist and nanobody (8, 10, 14, 19, 22). Our two methionine probes, Met-115$^{3.41}$ and Met-203$^{5.57}$ retain similar ligand-induced behavior in α_{1A}-AR-A4–active compared with α_{1A}-AR-A4 and α_{1A}-AR-A4 (L312F), where the latter are both essentially inactive. The chemical shift and line-broadening trends of Met-115$^{3.41}$ and Met-203$^{5.57}$ suggest that the transmission switch and DRY motif, in the presence of an inactive NP*XX*Y motif, can independently adopt conformations representative of active and inactive states. To fully adopt the conformational signatures of an active receptor, a functional NP*XX*Y motif is required (in α_{1A}-AR-A4–active) thus increasing the dynamics of the transmission switch and DRY motif, suggesting that the interdependence of the three microswitches is a consequence of their dynamic nature, and that this is required for full receptor function.

Although the striking linear chemical shift dependence for the $^{13}C^{\epsilon}H_3$ of Met-203$^{5.57}$ on ligand efficacy is consistent with a smooth change in equilibria from inactive to active, linear trends for $^{13}C^{\epsilon}H_3$ of Met-115$^{3.41}$ were less clear. In the inactive variants α_{1A}-AR-A4 and α_{1A}-AR-A4 (L312F) the resonance for apo, inverse agonist, and neutral antagonist shows little variation, but clear chemical shift changes and broadening are observed for agonists. The most distinct changes for the $^{13}C^{\epsilon}H_3$ of Met-115$^{3.41}$ were for α_{1A}-AR-A4–active, where in the apo state two peaks were consistently observed, suggesting slow exchange (> millisecond) between two distinct states, to which we attribute to restoring the NP*XX*Y microswitch. On the basis of chemical shift, we propose that the upfield peak of apo α_{1A}-AR-A4–active represents fully inactive receptor (state A in Fig. 6), expected for full inverse agonists, and the downfield peak with a basal state receptor that is stabilized by the neutral antagonist (state B in Fig. 6). This downfield "basal" peak shows approximate linear efficacy-dependent chemical shift changes with agonist titrations. Therefore, the $^{13}C^{\epsilon}H_3$ of Met-115$^{3.41}$ reflects three states, inactive (inverse agonist), an intermediate (basal), and active states (state(s) C in Fig. 6), where the latter progressively shift from partial to full agonist states. Interestingly, in a [$^{13}C^{\epsilon}H_3$]methionine-labeled study on the M2R, Met-112$^{3.41}$, which is equivalent to Met-115$^{3.41}$ in α_{1A}-AR, did not display efficacy-dependent chemical shift changes. In the presence of ligands, however, M2R Met-112$^{3.41}$ was resolved as two separate resonances, consistent with a slow exchanging microswitch (22) and may highlight some differences between how different rhodopsin family GPCRs function.

In this NMR study, by starting with a signaling incompetent variant of α_{1A}-AR and subsequently restoring signaling activity through back-mutations, we were able to study the functional dynamics of the key GPCR microswitches and how different ligands modulate this. Our NMR data for the transmission and DRY microswitches revealed ligand efficacy-dependent changes to the microswitch conformational equilibria, supporting a conformational selection mechanism for α_{1A}-AR modulation. This and the agonist-driven line broadening for both microswitches suggest similar mechanistic actions on the different microswitches, supporting ligand-driven allosteric communication between the microswitches. MD simulations (41) of β_2-AR suggest that these microswitches behaved independently of each other, with only loose allosteric coupling. Although this may be true over the relatively short timescales of

MD, we believe that over the course of an NMR experiment such loose allosteric coupling culminates in significant coupled shifts to the microswitch conformations and that this is likely how ligands modulate GPCR signaling in cells.

Experimental procedures

α_{1A}-AR constructs

The α_{1A}-AR-A4 variant is a thermostabilized human α_{1A}-AR, containing 15 stabilizing mutations (32). Met-$80^{2.58}$ in the spectra was introduced through the stabilization process in lieu of the naturally occurring amino acid leucine. As compared with WT, the C termini of the α_{1A}-AR-A4 variant was modified by truncation at Ser-351 and addition of a deca-His tag to facilitate purification (Fig. S1). For expression, the α_{1A}-AR variants sequences were subcloned into the pQE30-derived vector, pDS15, with a maltose-binding protein and a methionine-free monomeric ultrastable GFP (−Met-muGFP) (42) attached, respectively, to the N and C termini of the receptor via HRV 3C protease-cleavage sites. For the purpose of KingFisher-binding assays, α_{1A}-AR variants were subcloned into a similar vector, pDS11, in which muGFP was replaced with mCherry because the excitation and emission wavelengths of fluorescent QAPB were overlapping with those of GFP. The final sequence of α_{1A}-AR-A4 after purification (with residues left from HRV 3C cleavage) is: GPGSVFLSGNASDSSNSIQPPAPVNISKAILLGVILGGIILFGVLGNILVILSVACHRHLHSVTHYYVVYLAVADLLLTSTVMPFSAIYEVLGYWAFGRVFCNIWAAVDVLCCTASIMGLCIISIDRYIAVSYPLRYPTIVTQRRALMALLCVFALSLVISIGPLFGWRQPAPVDETICQINEEPGYVLFSALGSFYLPLAIILVMYCRVYVVAKRESRGLKSGLKTDKSDSEQVTLRIHRKNAPAGGSGMASAKTKTHFSVRLLKFSREKKAAKTLGIVVGCFVLCWLPFFLVMPIGSFFPDFKPSETVFKIVLWLGYLNSCIKPIIYLCYSQEFKKAFQNVLRIQCLCRKQSASHHHHHHHHHHGTRSLRGGLEVLFQ.

In the α_{1A}-AR-A4 (L312F) variant one stabilizing mutation Leu-312 was reversed to phenylalanine to improve the affinity of ligands compared with α_{1A}-AR-A4. α_{1A}-AR-A4–active (Y67N, K322N) is a signaling competent variant in which the two stabilizing mutations Tyr-67 and Lys-322 were reverted to the WT asparagines. α_{1A}-AR-A4 was used for NMR assignment, where each methionine was substituted to either leucine or isoleucine. All mutations were introduced through site-directed mutagenesis using PrimeSTAR DNA polymerase (TaKaRa).

α_{1A}-AR expression

All α_{1A}-AR variants were expressed in *E. coli* C43 (DE3) cells (Lucigen, Middleton, WI). For [$^{13}C^{\epsilon}H_3$]methionine-labeled expressions, 5 ml of LB pre-culture containing 100 mg/liter of ampicillin and 1% (w/v) glucose was inoculated with a single colony of C43 cells freshly transformed with the expression plasmid and incubated at 37 °C, 225 rpm for approximately 8 h. 2 ml of the LB day culture was centrifuged (1700 × *g*, 22 °C, 5 min) and the pellet was used to inoculate 100 ml of a defined minimal medium (M1 medium) (34) as overnight pre-culture. 10 ml of the overnight pre-culture was used to inoculate 500 ml of M1 medium in 2-liter flasks. The expression cultures were incubated at 37 °C, 225 rpm to reach OD_{600} of 0.6, at which point 50 mg/liter of [$^{13}C^{\epsilon}H_3$]methionine (Cambridge Stable Isotopes) was added along with 100 mg/liter of each lysine, threonine, phenylalanine, and 50 mg/liter of each leucine, isoleucine, and valine. The flasks were transferred to 20 °C and left shaking for 15 min prior to inducing protein expression with 250 μM isopropyl β-D-1-thiogalactopyranoside. After overnight expression (15–18 h, 20 °C, 225 rpm), the culture was harvested by centrifugation (2600 × *g*, 4 °C, 15 min). The final pellet was snap frozen in liquid nitrogen and stored at −80 °C. For unlabeled expression 5 ml of LB pre-culture was used to inoculate 500 ml of 2YT medium containing 100 mg/liter of ampicillin and 0.4% (w/v) glucose. At OD_{600} of 0.6 the culture was chilled on ice for 2 min prior to inducing protein expression with 250 μM isopropyl β-D-1-thiogalactopyranoside overnight and harvesting was carried out as described above.

α_{1A}-AR purification

The frozen cell pellet was thawed at room temperature for 30 min. A 10-ml pellet was gently resuspended in 40 ml of ice-cold solubilization buffer (25 mM HEPES, pH 7.5, 200 mM NaCl, 10% glycerol, 1% DDM (Anatrace), 0.12% cholesterol hemisuccinate (Anatrace), 0.6% CHAPS (Sigma), 50 mg of lysozyme, 5 mg of DNase, one tablet of EDTA-free complete protease inhibitor mixture (Roche Applied Science), 0.2–0.4 mM phenylmethylsulfonyl fluoride, and incubated on a turning wheel for 30 min at 4 °C. The cell membranes were then disrupted by a sonication device (Diagenode Bioruptor Plus, high power, 10 s on/20 s off for 30 cycles) followed by another 1-h incubation at 4 °C on the turning wheel. The cell debris was removed by centrifugation (12,000 × *g*, 4 °C, 40 min) and the supernatant was filtered using a 45-μm Durapore syringe filter (Merck Millipore). The cleared cell lysate was incubated with 3 ml of Talon metal affinity resin pre-equilibrated with 45 ml of equilibrium buffer (20 mM HEPES, pH 7.5, 300 mM NaCl, 10% glycerol, 0.05% DDM). After 1.5 h incubation at 4 °C, the resin retaining the receptor was washed three times with washing buffer 1 (20 mM HEPES, pH 7.5, 500 mM NaCl, 10% glycerol, 0.05% DDM) and then the full-length protein was eluted by 30 ml of elution buffer (20 mM HEPES, pH 7.5, 300 mM NaCl, 10% glycerol, 0.05% DDM, 250 mM imidazole). The eluate was concentrated down to 0.5–1 ml using a 100-kDa cut-off centrifugal filter device (Amicon Ultra, Millipore). Imidazole was removed by using a PD10 desalting column (GE Healthcare). Cleavage of fusion proteins from the receptor was carried out overnight at 4 °C by adding 100 mM Na_2SO_4, 1 mM tris(2-carboxyethyl)phosphine, and 300 pmol of glutathione *S*-transferase-tagged HRV 3C protease (made in house).

The cleaved mixture was incubated for 1 h with 2 ml of pre-equilibrated Talon resin. The resin was washed using 30 ml of washing buffer 2 (20 mM HEPES, pH 7.5, 300 mM NaCl, 10% glycerol, 0.05% DDM, 30 mM imidazole) and the receptor was eluted by 20 ml of elution buffer. The eluate was concentrated down to 450 μl by a 30-kDa cut-off centrifugal filter device (Amicon Ultra, Millipore) and was loaded onto a Superdex 200 10/300 increase column (GE Healthcare) equilibrated with size exclusion chromatography buffer (50 mM sodium phosphate, pH 7.5, 100 mM NaCl, 0.02% DDM). Size exclusion chromatography was carried out at a flow rate of 0.5 ml/min. The peak

fractions containing receptor were pooled and concentrated down to 100 μl using a 30-kDa cut-off centrifugal filter device (Amicon Ultra, Millipore). The sample buffer was exchanged twice to NMR buffer (50 mM sodium phosphate, pH 7.5, 100 mM NaCl, 99.9% D_2O). Yields were generally between 0.5 and 1 mg of receptor/liter of expression culture. Protein concentration was measured by BCA protein assay (Pierce, ThermoFisher).

NMR spectroscopy

NMR samples were prepared to 130 μl at 40–60 μM receptor in 3-mm Shigemi NMR tubes (Shigemi Inc., Allison Park, PA). Ligands were added at saturating concentrations that were 2 mM adrenaline for α_{1A}-AR-A4 and α_{1A}-AR-A4 (active), 400 μM prazosin, and 1 mM of other ligands to all mutants (Table S1). Adrenaline was supplemented with 1 mM of the antioxidant ascorbic acid. Samples containing low affinity agonists (phenylephrine and adrenaline) were recycled via competition with high affinity ligands, exchange was judged via the chemical shift of the Met-292$^{6.55}$ resonance. Experiments on α_{1A}-AR-A4 and α_{1A}-AR-A4-L312F, apo, and all ligands were performed at least twice on independent receptor samples (biological replicates), except WB-4101 and phentolamine, which were acquired once. Experiments on apo α_{1A}-AR-A4–active and bound to prazosin, silodosin, and oxymetazoline were performed at least twice on independent receptor samples, and for other ligands were performed once.

All NMR spectra were collected at 25 °C on an 800-MHz Bruker Avance II spectrometer equipped with a triple resonance cryoprobe. 2D ^{1}H-^{13}C SOFAST-HMQC (43) spectra were recorded by excitation with a 2.25-ms PC9 120° ^{1}H pulse and refocusing with a 1-ms r-SNOB shaped 180° ^{1}H pulse. The spectral widths were set to 12 and 25 ppm for ^{1}H and ^{13}C dimensions, respectively. For the spectra recorded for α_{1A}-AR-A4 variant (Fig. 2 and Fig. S3), 1024 × 128 complex points were recorded with a 25% Poisson-gap sampling schedule and 2048 scans; an acquisition time of 8.5 h. For the other spectra, 1024 × 200 complex points were recorded with either traditional or 60% Poisson-gap sampling schedule and 368 scans resulting in acquisition times of 10 and 6 h, respectively. Spectra were reconstructed with compressed sensing using qMDD and processed using NMRpipe (44) where data were multiplied by cosine bell functions and zero-filled once in each dimension. Spectra were analyzed in NMRFAM-Sparky (45) (Goddard, T. D. and Kneller, D. G., University of California, San Francisco).

The average chemical shift differences, $\Delta\delta$, were normalized using the equation $\Delta\delta = [(\Delta\delta_{1H})^2 + (\Delta\delta_{13C}/3.5)^2]^{0.5}$. The error values were calculated by the formula $|[\Delta\delta_{1H} \times R_{1H} + \Delta\delta_{13C} \times R_{13C}/(3.5)^2]|/\Delta\delta$, where R_{1H} and R_{13C} are the digital resolutions in ppm in the ^{1}H and ^{13}C dimensions, respectively (5).

Saturation and competition-binding assays

1 nmol of purified full-length α_{1A}-AR variant (mCherry attached) was resuspended in 10 ml of assay buffer (20 mM HEPES, pH 7.5, 100 mM NaCl, 0.02% DDM) and immobilized onto 200 μl of Dynabeads (Streptavidin T1) for 30 min at 4 °C. 100 μl of the suspension-containing beads with immobilized receptor were aliquoted to a 96-Deep Well plate from which the beads were transferred to another 96-Deep Well plate containing 100 μl of ligand solution using a KingFisher Flex magnetic particle processor. For saturation binding, immobilized receptors in each well were incubated with 100 μl of assay buffer containing increased concentrations (0, 3.125, 6.25, 12.5, 25, 50, 100, and 200 nM) of QAPB (quinazoline piperazine BODIPY) for 2 h at 22 °C. Nonspecific binding was determined by repeating the experiment in the presence of 10 μM prazosin. For competition binding, immobilized receptors were incubated with 100 μl of assay buffer containing 10 nM QAPB with the addition of ligands at various concentrations, as shown in supporting Figs. S5 and S8, for 2 h at 22 °C. Immobilized receptors were subsequently washed with 200 μl of assay buffer and resuspended in 100 μl of assay buffer. 90 μl of the final beads solution was transferred to a 96-well Greiner Bio-One nonbinding black plate. Fluorescence of bound QAPB was measured using a POLARstar OMEGA plate reader (BMG Labtech, Ortenburg, Germany) and normalized to mCherry fluorescence, which was detected simultaneously. Data represent the mean ± S.D. of three independent biological replicate experiments each performed in duplicate technical measurements. To compare ligand-binding affinities at α_{1A}-AR-A4 (L312F) and α_{1A}-AR-A4–active of α_{1A}-AR-A4, raw data from our previously published paper (32), were reanalyzed and presented in Table S1.

Thermostability assay

1 nM purified full-length α_{1A}-AR-A4 or α_{1A}-AR-A4–active (mCherry attached) was prepared in base buffer (20 mM HEPES, 100 mM NaCl, 0.1% DDM). To measure thermostability of receptors in the apo state, 100 μl of receptor solution was aliquoted into 24 wells of a 96-well PCR plate. 10 of the 12 duplicates were heated in gradient temperatures for 30 min and the two remaining duplicates were left at 4 °C for normalization. After thermo-treatment, the receptors were transferred to a KingFisher 96-Deep Well plate containing 2 μl of paramagnetic Dynabeads per well (streptavidin T1, ThermoFisher Scientific). The following few steps were automatically performed by using a KingFisher 96 magnetic particle processor. The receptor was first incubated with magnetic beads for 30 min at 4 °C. Then, magnetic beads were transferred to another 96-Deep Well plate containing 100 μl of ligand solution (20 mM HEPES, 100 mM NaCl, 0.1% DDM, 100 nM QAPB). The nonspecific binding was determined by competing QAPB with 100 μM of prazosin. After 1.5 h incubation, immobilized receptors were subsequently washed with 200 μl of assay buffer and resuspended in 100 μl of assay buffer. 90 μl of the final beads solution was transferred to a 96-well Greiner Bio-One nonbinding black plate. Fluorescence of bound QAPB was measured using a POLARstar OMEGA plate reader (BMG Labtech, Ortenburg, Germany) and normalized to mCherry fluorescence, which was detected simultaneously. To measure the thermostability of α_{1A}-AR variants in the presence of ligand, receptors were preincubated with 100 nM QAPB for 1 h on ice prior to being heated at varying temperatures. The remaining steps were carried out as described for apo state thermostability assay. Data represent the mean ± S.D. of three independent biological replicate experiments each performed in duplicate technical replicate measurements.

IP_1 assay

$G\alpha_{q/11}$ signaling assays were carried out using the IP-One HTRF® Assay Kit (Cisbio Bioassays, France) measuring IP_1 using the manufacturer's protocol. COS-7 cells were seeded at 25,000 cells per well in a 96-well plate and incubated overnight at 37 °C and 5% CO_2 in Dulbecco's modified Eagle's medium (DMEM) (Gibco, Gaithersburg, MD) supplemented with 10% fetal bovine serum (FBS) (Scientifix Life, Melbourne, Australia), 1% L-glutamine (Gibco), and 1% penicillin/streptomycin (Gibco). Cells were transfected with pcDNA3.1 constructs of WT or mutant α_{1A}-ARs using Lipofectamine 2000 (Invitrogen) at 0.25 μg of DNA/well. 24 h later, cells were stimulated with ligands for 2 h at 37 °C in 40 μl of Stimulation Buffer, then frozen at −80 °C. 14 μl of thawed sample were transferred to a white HTRF® 384-well Optiplate (PerkinElmer Life Sciences), incubated with development reagents in the dark for 1 h with shaking, and analyzed by time-resolved fluorescence using a POLARstar OMEGA plate reader (BMG Labtech, Ortenburg, Germany). Data were analyzed against the kit's standard curve. Data represent mean ± S.D. of three independent biological replicate experiments (except for some samples in the screening assay in Fig. S8, where some receptors were measured only once or twice). For each biological replicate samples were measured in triplicate technical replicate measurements, unless otherwise stated in the figure legends (as in Fig. S8).

NanoBiT G protein activity assay

COS-7 cells grown in 10% FBS, 1% L-glutamine, 1% penicillin/streptomycin, DMEM were seeded at 250,000 cells/well on a 6-well–plate. Cells were then transiently co-transfected in the 6-well–plate, with 0.1 μg of $G\alpha_q$-LgBiT (GNAQ-11S) DNA, 0.5 μg of Gβ-untagged (GNB1) DNA, 0.5 μg of Gγ-SmBiT (114-GnG_2) DNA, 0.2 μg of Guanine Release Factor (RIC8A) DNA, and 0.5 μg of α_{1A}-AR (or respective AR mutants) DNA using Lipofectamine 2000 transfection reagent as per the manufacturer's instructions. The next day the cells were resuspended in phenol red-free DMEM containing 10% FBS, 1% L-glutamine, 1% penicillin/streptomycin, 25 mM HEPES and seeded at 50,000 cells/well to a white 96-well–plate and incubated overnight. On the day of the assay, plates were preincubated with 10 μM furimazine for 1 h. Following incubation, raw luminescence counts in each well were measured every 12 s over the course of the assay using a POLARstar Omega plate reader (BMG Labtech). Cells were treated with either vehicle or a saturating concentration of each ligand (50 nM for A-61603 and 100 nM for antagonists). Luminescence counts were plotted against time, with the final preincubation reading assigned as the zero-time point (time of vehicle/ligand addition). A baseline correction was then performed by subtracting the luminescence counts in the vehicle-treated samples from the ligand-treated samples, which resulted in a time course plot of ligand-induced luminescence counts. Initial raw luminescence counts were used as a readout of G protein expression levels. Data represent the mean ± S.E. of three independent biological replicate experiments each performed in triplicate technical replicate measurements, unless otherwise stated in the figure legends.

Intracellular Ca^{2+} mobilization assays

COS-7 cells were seeded in 10-cm culture dishes at 3×10^6 cells/dish and allowed to grow overnight at 37 °C, 5% CO_2 in DMEM supplemented with 10% FBS, 1% L-glutamine, and 1% penicillin/streptomycin (Life Technologies). The next day the cells were transfected with 30 μg of receptor DNA construct (pcDNA3.1 expression vector containing WT or mutant α_{1A}-ARs) using 60 μl of Lipofectamine 2000 (Invitrogen) transfecting reagent per dish. The following day, cells were transferred to 96-well– culture plates (5×10^4 cells/well) and allowed to grow overnight. On the day of the experiment cells were washed twice with Ca^{2+} assay buffer (150 mM NaCl, 2.6 mM KCl, 1.2 mM $MgCl_2$, 10 mM D-glucose, 10 mM HEPES, 2.2 mM $CaCl_2$, 0.5% (w/v) BSA, and 4 mM probenecid, pH 7.4) and incubated in Ca^{2+} assay buffer containing 1 mM Fluo-4-AM for 1 h in the dark at 37 °C and 5% CO_2. After two washes with Ca^{2+} assay buffer, fluorescence was measured for 1.5 min upon the addition of ligands in a Flexstation 3 (Molecular Devices, Sunnyvale, CA) using an excitation wavelength of 485 nm and emission wavelength of 520 nm. Data were normalized to the peak response elicited by 3 μM ionomycin (Life Technologies). Data represent the mean ± S.D. of three independent biological replicate experiments each performed in triplicate technical replicate measurements, unless otherwise stated in the figure legends.

Homology modeling

Homology models of inactive and active state α_{1A}-AR were built with I-TASSER (46) using crystal structures of β_2-AR as the templates, which show 23% identity and 39% similarity. For inactive state models, the structure of β_2-AR bound to the antagonist carazolol and the inactive state stabilizing nanobody, Nb60 (PDB ID 5JQH) (47), was used as a template. For the active state models, the crystal structure of a β_2-AR–Gs protein complex bound to the agonist BI-167107 (PDB ID 3SN6) (48) was used as a template. The N- and C-terminal regions as well as the ICL3 regions, which have no sequence similarity to the template, were deleted from the model. Energy minimization was performed using Minimize tool in Maestro version 11.7.012 (Schrödinger, Inc.) under OPLS 2005 (49) forcefield.

Data availability

All data generated or analyzed during this study are included in the published article (and supporting information).

Author contributions—F.-J. W., A. A.-R., R. A. B., D. J. S., and P. R. G. data curation; F.-J. W. formal analysis; F.-J. W., L. M. W., A. A.-R., A. G., T. M. V. , M. K., A. R. W., M. D. G., and P. R. G. investigation; F.-J. W. methodology; F.-J. W. writing-original draft; F.-J. W., L. M. W., A. A.-R., A. G., T. M. V., M. K., A. R. W., M. D. G., R. A. B., D. J. S., and P. R. G. writing-review and editing; A. A.-R., A. R. W., M. D. G., R. A. B., D. J. S., and P. R. G. conceptualization; A. A.-R., M. D. G., R. A. B., D. J. S., and P. R. G. resources; A. A.-R., A. R. W., M. D. G., R. A. B., D. J. S., and P. R. G. supervision; A. A.-R., M. D. G., R. A. B., D. J. S., and P. R. G. funding acquisition; A. A.-R., R. A. B., D. J. S., and P. R. G. project administration.

Acknowledgments—We thank Dr. Fabian Bumbak (The Florey Institute of Neuroscience and Mental Health) for assistance with optimizing the expression and purification of receptor samples; Prof. Dmitry Veprintsev (University of Nottingham) and Dr. Franziska Heydenreich (Stanford University) for suggesting back-mutations for the generation of α_{1A}-AR-A4–active; Prof. Asuka Inoue (Tohoku University) for supplying plasmids for the G protein activity assays; Sharon Layfield (The Florey Institute of Neuroscience and Mental Health) and Dr. Ashish Sethi (The University of Melbourne) for assistance with cell-based assays and NMR data analysis, respectively; Dr. David Chalmers (Monash University) and the Monash University Medicinal Chemistry Computational Chemistry Facility for the assistance with computational modeling; and The Bio21 NMR facility for access to spectrometers.

References

1. Manglik, A., and Kruse, A. C. (2017) Structural basis for G protein-coupled receptor activation. *Biochemistry* **56,** 5628–5634 CrossRef Medline
2. Carpenter, B., and Tate, C. G. (2017) Active state structures of G protein-coupled receptors highlight the similarities and differences in the G protein and arrestin coupling interfaces. *Curr. Opin. Struct. Biol.* **45,** 124–132 CrossRef Medline
3. García-Nafría, J., and Tate, C. G. (2019) Cryo-EM structures of GPCRs coupled to Gs, Gi, and Go. *Mol. Cell. Endocrinol.* **488,** 1–13 CrossRef Medline
4. Bokoch, M. P., Zou, Y., Rasmussen, S. G., Liu, C. W., Nygaard, R., Rosenbaum, D. M., Fung, J. J., Choi, H. J., Thian, F. S., Kobilka, T. S., Puglisi, J. D., Weis, W. I., Pardo, L., Prosser, R. S., Mueller, L., and Kobilka, B. K. (2010) Ligand-specific regulation of the extracellular surface of a G-protein-coupled receptor. *Nature* **463,** 108–112 CrossRef Medline
5. Kofuku, Y., Ueda, T., Okude, J., Shiraishi, Y., Kondo, K., Maeda, M., Tsujishita, H., and Shimada, I. (2012) Efficacy of the β_2-adrenergic receptor is determined by conformational equilibrium in the transmembrane region. *Nat. Commun.* **3,** 1045 CrossRef Medline
6. Liu, J. J., Horst, R., Katritch, V, Stevens, R. C., Wüthrich, K. (2012) Biased signaling pathways in β_2-AR characterized by ^{19}F-NMR. *Science* **335,** 1106–1110 CrossRef Medline
7. Horst, R., Liu, J., Stevens, R., and Wüthrich, K. (2013) β2-adrenergic receptor activation by agonists studied with 19F NMR spectroscopy. *Angew. Chem.* **125,** 10962–10965 CrossRef
8. Nygaard, R., Zou, Y., Dror, R. O., Mildorf, T. J., Arlow, D. H., Manglik, A., Pan, A. C., Liu, C. W., Fung, J. J., Bokoch, M. P., Thian, F. S., Kobilka, T. S., Shaw, D. E., Mueller, L., Prosser, R. S., and Kobilka, B. K. (2013) The dynamic process of β_2-adrenergic receptor activation. *Cell* **152,** 532–542 CrossRef Medline
9. Kofuku, Y., Ueda, T., Okude, J., Shiraishi, Y., Kondo, K., Mizumura, T., Suzuki, S., and Shimada, I. (2014) Functional dynamics of deuterated β_2-adrenergic receptor in lipid bilayers revealed by NMR spectroscopy. *Angew. Chem. Int. Ed. Engl.* **53,** 13376–13379 CrossRef Medline
10. Manglik, A., Kim, T. H., Masureel, M., Altenbach, C., Yang, Z., Hilger, D., Lerch, M. T., Kobilka, T. S., Thian, F. S., Hubbell, W. L., Prosser, R. S., and Kobilka, B. K. (2015) Structural insights into the dynamic process of β_2-adrenergic receptor signaling. *Cell* **161,** 1101–1111 CrossRef Medline
11. Eddy, M. T., Didenko, T., Stevens, R. C., and Wüthrich, K. (2016) β_2-Adrenergic receptor conformational response to fusion protein in the third intracellular loop. *Structure* **24,** 2190–2197 CrossRef Medline
12. Kobilka, B., Gether, U., Seifert, R., Lin, S., and Ghanouni, P. (1999) Characterization of ligand-induced conformational states in the β_2-adrenergic receptor. *J. Recept. Signal. Transduct. Res.* **19,** 293–300 CrossRef Medline
13. Isogai, S., Deupi, X., Opitz, C., Heydenreich, F. M., Tsai, C. J., Brueckner, F., Schertler, G. F., Veprintsev, D. B., and Grzesiek, S. (2016) Backbone NMR reveals allosteric signal transduction networks in the β_1-adrenergic receptor. *Nature* **530,** 237–241 CrossRef Medline
14. Solt, A. S., Bostock, M. J., Shrestha, B., Kumar, P., Warne, T., Tate, C. G., and Nietlispach, D. (2017) Insight into partial agonism by observing multiple equilibria for ligand-bound and Gs-mimetic nanobody-bound β_1-adrenergic receptor. *Nat. Commun.* **8,** 1795 CrossRef Medline
15. Ye, L., Van Eps, N., Zimmer, M., Ernst, O. P., and Prosser, R. S. (2016) Activation of the A2A adenosine G-protein-coupled receptor by conformational selection. *Nature* **533,** 265–268 CrossRef Medline
16. Clark, L. D., Dikiy, I., Chapman, K., Rödström, K. E., Aramini, J., LeVine, M. V., Khelashvili, G., Rasmussen, S. G., Gardner, K. H., and Rosenbaum, D. M. (2017) Ligand modulation of sidechain dynamics in a wild-type human GPCR. *Elife* **6,** e28505 CrossRef Medline
17. Ye, L., Neale, C., Sljoka, A., Lyda, B., Pichugin, D., Tsuchimura, N., Larda, S. T., Pomès, R., García, A. E., Ernst, O. P., Sunahara, R. K., and Prosser, R. S. (2018) Mechanistic insights into allosteric regulation of the A2A adenosine G protein-coupled receptor by physiological cations. *Nat. Commun.* **9,** 1372 CrossRef Medline
18. Eddy, M. T., Lee, M. Y., Gao, Z. G., White, K. L., Didenko, T., Horst, R., Audet, M., Stanczak, P., McClary, K. M., Han, G. W., Jacobson, K. A., Stevens, R. C., and Wüthrich, K. (2018) Allosteric coupling of drug binding and intracellular signaling in the A2A adenosine receptor. *Cell* **172,** 68–80.e12 CrossRef Medline
19. Sounier, R., Mas, C., Steyaert, J., Laeremans, T., Manglik, A., Huang, W., Kobilka, B. K., Démené, H., and Granier, S. (2015) Propagation of conformational changes during μ-opioid receptor activation. *Nature* **524,** 375–378 CrossRef Medline
20. Okude, J., Ueda, T., Kofuku, Y., Sato, M., Nobuyama, N., Kondo, K., Shiraishi, Y., Mizumura, T., Onishi, K., Natsume, M., Maeda, M., Tsujishita, H., Kuranaga, T., Inoue, M., and Shimada, I. (2015) Identification of a conformational equilibrium that determines the efficacy and functional selectivity of the μ-opioid receptor. *Angew. Chem. Int. Ed. Engl.* **54,** 15771–15776 CrossRef Medline
21. Casiraghi, M., Damian, M., Lescop, E., Point, E., Moncoq, K., Morellet, N., Levy, D., Marie, J., Guittet, E., Banères, J. L., and Catoire, L. J. (2016) Functional modulation of a G protein-coupled receptor conformational landscape in a lipid bilayer. *J. Am. Chem. Soc.* **138,** 11170–11175 CrossRef Medline
22. Xu, J., Hu, Y., Kaindl, J., Risel, P., Hübner, H., Maeda, S., Niu, X., Li, H., Gmeiner, P., Jin, C., and Kobilka, B. K. (2019) Conformational complexity and dynamics in a muscarinic receptor revealed by NMR spectroscopy. *Mol. Cell* **75,** 53–65.e7 CrossRef Medline
23. Shimada, I., Ueda, T., Kofuku, Y., Eddy, M. T., and Wüthrich, K. (2019) GPCR drug discovery: integrating solution NMR data with crystal and cryo-EM structures. *Nat. Rev. Drug Discov.* **18,** 59–82 Medline CrossRef
24. Deupi, X., and Standfuss, J. (2011) Structural insights into agonist-induced activation of G-protein-coupled receptors. *Curr. Opin. Struct. Biol.* **21,** 541–551 CrossRef Medline
25. Trzaskowski, B., Latek, D., Yuan, S., Ghoshdastider, U., Debinski, A., and Filipek, S. (2012) Action of molecular switches in GPCRs: theoretical and experimental studies. *Curr. Med. Chem.* **19,** 1090–1109 CrossRef Medline
26. Ahuja, S., and Smith, S. O. (2009) Multiple switches in G protein-coupled receptor activation. *Trends Pharmacol. Sci.* **30,** 494–502 CrossRef Medline
27. Bhattacharya, S., and Vaidehi, N. (2014) Differences in allosteric communication pipelines in the inactive and active states of a GPCR. *Biophys. J.* **107,** 422–434 CrossRef Medline
28. Latorraca, N. R., Venkatakrishnan, A. J., and Dror, R. O. (2017) GPCR dynamics: structures in motion. *Chem. Rev.* **117,** 139–155 CrossRef Medline
29. Akinaga, J., García-Saínz, J. A., and S. Pupo, A. (2019) Updates in the function and regulation of α1-adrenoceptors. *Br. J. Pharmacol.* **176,** 2343–2357 Medline
30. Perez, D. M., and Doze, V. (2011) Cardiac and neuroprotection regulated by α_1-adrenergic receptor subtypes. *J. Recept. Signal Transduct. Res.* **31,** 98–110 CrossRef Medline
31. Scott, D. J., and Plückthun, A. (2013) Direct molecular evolution of detergent-stable G protein-coupled receptors using polymer encapsulated cells. *J. Mol. Biol.* **425,** 662–677 CrossRef Medline
32. Yong, K. J., Vaid, T. M., Shilling, P. J., Wu, F. J., Williams, L. M., Deluigi, M., Plückthun, A., Bathgate, R. A. D., Gooley, P. R., and Scott, D. J. (2018) Determinants of ligand subtype-selectivity at α1A-adrenoceptor revealed

using saturation transfer difference (STD) NMR. *ACS Chem. Biol.* **13,** 1090–1102 CrossRef Medline

33. Isberg, V., de Graaf, C., Bortolato, A., Cherezov, V., Katritch, V., Marshall, F. H., Mordalski, S., Pin, J.-P., Stevens, R. C., Vriend, G., and Gloriam, D. (2015) Generic GPCR residue numbers: aligning topology maps while minding the gaps. *Trends Pharmacol. Sci.* **36,** 22–31 CrossRef Medline
34. Bumbak, F., Keen, A. C., Gunn, N. J., Gooley, P. R., Bathgate, R. A. D., and Scott, D. J. (2018) Optimization and $^{13}CH_3$ methionine labeling of a signaling competent neurotensin receptor 1 variant for NMR studies. *Biochim. Biophys. Acta* **1860,** 1372–1383 CrossRef
35. Bumbak, F., Bathgate, R. A. D., Scott, D. J., and Gooley, P. R. (2019) Expression and purification of a functional *E. coli* $^{13}CH_3$-methionine-labeled thermostable neurotensin receptor 1 variant for solution NMR studies. *Methods Mol. Biol.* **1947,** 31–55 CrossRef Medline
36. Hwa, J., Graham, R. M., and Perez, D. M. (1995) Identification of critical determinants of α_1-adrenergic receptor subtype selective agonist binding. *J. Biol. Chem.* **270,** 23189–23195 CrossRef Medline
37. Butterfoss, G. L., DeRose, E. F., Gabel, S. A., Perera, L., Krahn, J. M., Mueller, G. A., Zheng, X., and London, R. E. (2010) Conformational dependence of ^{13}C shielding and coupling constants for methionine methyl groups. *J. Biomol. NMR* **48,** 31–47 CrossRef Medline
38. Zhu, J., Taniguchi, T., Takauji, R., Suzuki, F., Tanaka, T., and Muramatsu, I. (2000) Inverse agonism and neutral antagonism at a constitutively active α-1A adrenoceptor. *Br. J. Pharmacol.* **131,** 546–552 CrossRef Medline
39. Inoue, A., Raimondi, F., Kadji, F. M. N., Singh, G., Kishi, T., Uwamizu, A., Ono, Y., Shinjo, Y., Ishida, S., Arang, N., Kawakami, K., Gutkind, J. S., Aoki, J., and Russell, R. B. (2019) Illuminating G-protein-coupling selectivity of GPCRs. *Cell* **177,** 1933–1947.e25 CrossRef Medline
40. Cotecchia, S., Schwinn, D. A., Randall, R. R., Lefkowitz, R. J., Caron, M. G., and Kobilka, B. K. (1988) Molecular cloning and expression of the cDNA for the hamster α1-adrenergic receptor. *Proc. Natl. Acad. Sci. U.S.A.* **85,** 7159–7163 CrossRef Medline
41. Dror, R. O., Arlow, D. H., Maragakis, P., Mildorf, T. J., Pan, A. C., Xu, H., Borhani, D. W., and Shaw, D. E. (2011) Activation mechanism of the β_2-adrenergic receptor. *Proc. Natl. Acad. Sci. U.S.A.* **108,** 18684–18689 CrossRef Medline
42. Scott, D. J., Gunn, N. J., Yong, K. J., Wimmer, V. C., Veldhuis, N. A., Challis, L. M., Haidar, M., Petrou, S., Bathgate, R. A. D., and Griffin, M. D. W. (2018) A novel ultra-stable, monomeric green fluorescent protein for direct volumetric imaging of whole organs using CLARITY. *Sci. Rep.* **8,** 667 CrossRef Medline
43. Schanda, P., Kupce, E., and Brutscher, B. (2005) SOFAST-HMQC experiments for recording two-dimensional heteronuclear correlation spectra of proteins within a few seconds. *J. Biomol. NMR* **33,** 199–211 CrossRef Medline
44. Delaglio, F., Grzesiek, S., Vuister, G. W., Zhu, G., Pfeifer, J., and Bax, A. (1995) NMRPipe: a multidimensional spectral processing system based on UNIX pipes. *J. Biomol. NMR* **6,** 277–293 Medline
45. Lee, W., Tonelli, M., and Markley, J. L. (2015) NMRFAM-SPARKY: enhanced software for biomolecular NMR spectroscopy. *Bioinformatics* **31,** 1325–1327 CrossRef Medline
46. Zhang, J., Yang, J., Jang, R., and Zhang, Y. (2015) GPCR-I-TASSER: a hybrid approach to G protein-coupled receptor structure modeling and the application to the human genome. *Structure* **23,** 1538–1549 CrossRef Medline
47. Staus, D. P., Strachan, R. T., Manglik, A., Pani, B., Kahsai, A. W., Kim, T. H., Wingler, L. M., Ahn, S., Chatterjee, A., Masoudi, A., Kruse, A. C., Pardon, E., Steyaert, J., Weis, W. I., Prosser, R. S., *et al.* (2016) Allosteric nanobodies reveal the dynamic range and diverse mechanisms of G-protein-coupled receptor activation. *Nature* **535,** 448–452 CrossRef Medline
48. Rasmussen, S. G., DeVree, B. T., Zou, Y., Kruse, A. C., Chung, K. Y., Kobilka, T. S., Thian, F. S., Chae, P. S., Pardon, E., Calinski, D., Mathiesen, J. M., Shah, S. T., Lyons, J. A., Caffrey, M., Gellman, S. H., *et al.* (2011) Crystal structure of the β_2 adrenergic receptor-Gs protein complex. *Nature* **477,** 549–555 CrossRef Medline
49. Siu, S. W., Pluhackova, K., and Böckmann, R. A. (2012) Optimization of the OPLS-AA force field for long hydrocarbons. *J. Chem. Theory Comput.* **8,** 1459–1470 CrossRef Medline